Combined effects of nonparaxiality, optical activity, and walk-off on rogue wave propagation in optical fibers filled with chiral materials

D. D. Estelle Temgoua,[1,2,3,*] M. B. Tchoula Tchokonte,[3,†] and T. C. Kofane[1,4,‡]

[1]*Laboratory of Mechanics, Materials and Structures, Post Graduate School in Sciences, Technology and Geosciences, Doctoral Research, Unit in Physics and Applications, University of Yaounde I, P.O. Box 812, Yaounde, Cameroon*

[2]*Organization for Women in Science for the Developing World, ICTP Campus, Strada Costiera 11, 34151 Trieste, Italy*

[3]*Department of Physics and Astronomy, University of the Western Cape, Private Bag X17, Bellville, 7535 South Africa*

[4]*Centre d'Excellence Africain en Technologies de l'Information et de la Communication, University of Yaounde I, P.O. Box 812, Yaounde, Cameroon*

(Received 30 October 2017; revised manuscript received 29 January 2018; published 9 April 2018)

The generalized nonparaxial nonlinear Schrödinger (NLS) equation in optical fibers filled with chiral materials is reduced to the higher-order integrable Hirota equation. Based on the modified Darboux transformation method, the nonparaxial chiral optical rogue waves are constructed from the scalar model with modulated coefficients. We show that the parameters of nonparaxiality, third-order dispersion, and differential gain or loss term are the main keys to control the amplitude, linear, and nonlinear effects in the model. Moreover, the influence of nonparaxiality, optical activity, and walk-off effect are also evidenced under the defocusing and focusing regimes of the vector nonparaxial NLS equations with constant and modulated coefficients. Through an algorithm scheme of wider applicability on nonparaxial beam propagation methods, the most influential effect and the simultaneous controllability of combined effects are underlined, showing their properties and their potential applications in optical fibers and in a variety of complex dynamical systems.

DOI: 10.1103/PhysRevE.97.042205

I. INTRODUCTION

After the investigation of fundamental problems of electromagnetic wave interaction with chiral materials, the area of wave propagation in chiral media has renewed attention both from theoretical and experimental points of view [1]. Chirality, which refers to the handedness of an object or a medium, has to play an important role in a variety of fields, including chemistry [2], optics [3], particle physics [4,5], and mathematics [6]. The electromagnetic wave propagation through such medium displays two unequal characteristic wave numbers for the right- and left-circularly polarized eigenmodes, which results in both optical activity and circular dichrosim, as consequences of the circular birefringence [1,7]. Significant advances have taken place on some aspects relating to the applications of chiral media. One can mention the wave-guiding structures filled with chiral materials, which show many interesting features through the integrated optic applications like directional couplers, which can be used as optical switches for energy transfer from one fiber to another adjacent one. In fact, chiral medium has many potentials and the development of integrated circuitry with chiral substrates and the multiplexing in chiral fibers are important progress with potential applications in optics [8,9].

In recent times, much attention has been focused on understanding of rogue wave propagation in optical fibers filled with chiral materials. The nature of rogue waves has been discussed in hydrodynamics [10–12] and initiated in nonlinear optics, by the pioneering measurement of Solli *et al.* [13] through the analysis of the supercontinuum generation in optical fibers, and later in a photonic crystal fiber [14]. Their occurrences have been later observed in optical cavities [15], optical wave guides [16], Bose-Einstein condensates [17–19], laser-plasma interactions [20], econophysics [21], and even in finance [22].

The concept of rogue waves which refers to rogons has been applied to pulses emerging from optical fibers, and both numerical simulations and experiments show that the probability of their generations increases with the increase of the initial noise level responsible for the modulation instability (MI) [23]. It is worth noting that the MI that leads to their generation evolves two distinct directions with opposite sense. On the one hand, it deals with the undesirable effects like the non-return-to-zero code in optical communication, the drastic enhancement of MI gain in the WDM (wavelength-division multiplexing) systems which sets the limitation of the bandwidth window of the communication system, MI lasers, and the new frequency generations of ultrashort pulses in optical systems. On the other hand, a suitable manipulation of MI has also found important applications in optical amplification of weak signal, dispersion management, optical switching, and the production of ultrashort pulses.

Despite multiple observations in many other fields, the origin and the predictability of rogons remains uncertain [24], as does the kind of MI that leads to rogue wave generation [25,26]. In fact, in optical communication systems [27–29], many works have been done with the objective of reducing the disastrous effects caused by MI. Important progress has been made very recently by Baronio *et al.* [30], who showed

*Corresponding author: estelletemgoua@yahoo.fr
†mtchokonte@uwc.ac.za
‡tckofane@yahoo.com

that the MI is a necessary but not a sufficient condition for the existence of rogue waves. Through their results, they confirmed that rogue waves can exist if and only if the MI gain band also contains the zero-frequency perturbation as a limiting case known as baseband MI.

In the context of adequate model, the focusing nonlinear Schrödinger (NLS) equation has played an important role of universal model for rogue waves description in both optics [31] and hydrodynamics [32] and, later on, in many physical systems [33,34]. Therefore, the nonparaxial NLS equation model was used in the literature by Baruch *et al.* [35] and Chamoro-Posada *et al.* [36]. Moreover, the development and testing of two alternative nonparaxial beam propagation methods investigated by Chamoro-Posada *et al.* [37] have provided the foundations upon which further investigations as the modeling of numerous higher-order effects and different physical geometries can now be undertaken with much greater confidence. Therefore, the difference-differential approach that is used in this work is flexible in the accommodation of additional effects. Furthermore, the same model has been used in the literature by many authors [38,39].

Then after many years, scientists [30,40] recognized that describing complex systems with the standard NLS equation is oversimplifying the nonlinear phenomena that can occur in those systems. As a consequence, this problem pushes researchers [41,42] to turn to higher-order NLS equations. Moreover, it was pointed out that the vector NLS equations describe rogue waves with higher accuracy than the scalar models [43–45]. Under this assumption, the existence of vector rogue waves in the defocusing regime was a crucial progress in the explanation of rogue waves in multicomponent systems [30].

Among different models that have been studied before, no report to the best of our knowledge is adequate to perform the description of the generation and the propagation of nonparaxial rogue waves in optical fibers filled with chiral materials. As we are working under the assumption of high intensity and beam narrowness, we investigated both scalar and vector models, which can be used efficiently to describe simultaneous effects of nonparaxiality, optical activity, and walk-off on rogue waves propagating in optical fibers, filled with chiral materials. As physical phenomena require modeling waves with two or more components to account for different modes, frequencies, or polarizations [7,43,46], it is also necessary to use the vector NLS equations, which allow energy transfer between components and which potentially yields rich and significant new families of vector rogue wave solutions.

As methodology of resolution of the higher-order nonparaxial chiral NLS equations derived in Appendix A, we use both similitude reduction and modified Darboux transformation (MDT) methods [47–49] to find the analytical solutions of the scalar model, and both difference-differential equation method and Darboux dressing transformation (DDT) methods [44,50–54] to find the numerical solutions of the vector model. Indeed, the properties of simultaneous controllability of nonparaxiality, optical activity, and walk-off effects on rogue waves are underlined.

The paper is organized as follows: In Sec. II we find under the boundedness condition the nonparaxial chiral optical rogue waves with modulated coefficients via the MDT method. In Sec. III we investigate the dynamical behavior and features of nonparaxial chiral optical rogue waves through their specific control parameters. In Sec. IV we analyze the influence of nonparaxiality, optical activity, and walk-off on the vector nonparaxial chiral NLS equations with constant coefficients. In Sec. V we present the influence of combined effects through the vector nonparaxial chiral NLS equations with modulated coefficients. In Sec. VI we summarize the outcomes.

II. SIMILARITY REDUCTION, FIRST- AND SECOND-ORDER NONPARAXIAL CHIRAL OPTICAL ROGUE WAVES WITH MODULATED COEFFICIENTS

To describe the optical rogue wave propagation in chiral media, we deduce from Eq. (A25), derived in Appendix A, the nonparaxial chiral NLS equation with modulated coefficients, in the form

$$d(\xi)\frac{\partial^2\psi}{\partial\xi^2} + j\frac{\partial\psi}{\partial\xi} + P(\xi,\tau)\frac{\partial^2\psi}{\partial\tau^2} - j\gamma(\xi)\frac{\partial^3\psi}{\partial\tau^3} + j\mu(\xi,\tau)\psi \mp D(\xi,\tau)\psi - C(\xi,\tau)|\psi|^2\psi + j\alpha_3(\xi)|\psi|^2\frac{\partial\psi}{\partial\tau} + \eta(\xi)\frac{\partial\psi}{\partial\tau} \pm j\sigma_3(\xi,\tau)\frac{\partial\psi}{\partial\tau} = 0, \quad (1)$$

where ξ is the propagation distance, and τ is the retarded time. The subscripts ξ and τ stand for partial differentiation. The variable coefficients $P(\xi,\tau)$, $\mu(\xi,\tau)$, $D(\xi,\tau)$, $C(\xi,\tau)$, and $\sigma_3(\xi,\tau)$ are related to the space- and time-modulated group-velocity dispersion (GVD), gain or loss term of the induced optical activity, linear birefringence, self-phase modulation (SPM), and linear group velocity or walk-off. Parameters $d(\xi)$, $\gamma(\xi)$, $\alpha_3(\xi)$, and $\eta(\xi)$ are related to the space-modulated nonparaxial parameter, TOD (third-order dispersion), SS (self-steepening), and the differential gain or loss term, respectively. Through Eq. (1), we can see the importance and the necessity to take into account those parameters which are responsible of nonparaxial, optical activity, and walk-off effects. These additional terms will help to improve the description and the control of rogue wave propagation under the above assumptions. As the assumption of controllability [55] is verified by the above model, we are going to find the rational solutions with variable coefficients which may be useful to control the propagation of the nonparaxial chiral optical rogue waves.

Modulated coefficients in Eq. (1) can strongly affect the wave propagation in chiral optical fiber because of the nonintegrability of the model. To solve this problem, we use the symmetry reduction method [56,57] to obtain some integrability conditions and to reduce the generalized nonparaxial chiral NLS equation to the higher-order integrable Hirota equation. So doing, we use the envelope field in the form [55,58,59]

$$\psi(\xi,\tau) = A(\xi)V[Z(\xi),T(\xi,\tau)]\exp\{i\rho(\xi,\tau)\}, \quad (2)$$

to construct the rational solutions related to nonparaxial chiral optical rogue waves, where $A(\xi)$ is the amplitude, $Z(\xi)$ the effective propagation distance, $T(\xi,\tau)$ the similitude variable, and $V[Z(\xi),T(\xi,\tau)]$ the complex field. The variable $\rho(\xi,\tau)$ is the phase of the wave. This form of envelope field is also known as the similarity transformation or the reduction method.

Substituting Eq. (2) into Eq. (1) gives a coupled system of partial differential equations with variable coefficients:

$$d(\xi)\big(A_{\xi\xi}V+2A_\xi Z_\xi V_Z+2A_\xi T_\xi V_T+2AZ_\xi T_\xi V_{ZT}+AZ_{\xi\xi}V_Z+AT_{\xi\xi}V_T+AZ_\xi{}^2V_{ZZ}+AT_\xi{}^2V_{TT}-A\rho_\xi{}^2V\big)$$
$$-AV\rho_\xi+P(\xi,\tau)\big(AV_{TT}T_\tau{}^2+AV_TT_{\tau\tau}-AV\rho_\tau{}^2\big)+\gamma(\xi)\big(3AV_TT_{\tau\tau}\rho_\tau+3AV_TT_\tau\rho_{\tau\tau}+3AV_{TT}T_\tau{}^2\rho_\tau$$
$$+AV\rho_{\tau\tau\tau}-AV\rho_\tau{}^3\big)\mp D(\xi,\tau)AV-C(\xi,\tau)A^2|V|^2AV-\alpha_3(\xi)A^2|V|^2AV\rho_\tau+\eta(\xi)AT_\tau V_T\mp\sigma(\xi,\tau)AV\rho_\tau=0, \quad (3)$$

$$d(\xi)(AV\rho_{\xi\xi}+2A_\xi\rho_\xi V+2AZ_\xi\rho_\xi V_Z+2A\rho_\xi T_\xi V_T)+A_\xi V+AV_ZZ_\xi+AV_TT_\xi+P(\xi,\tau)(AV\rho_{\tau\tau}+2AV_TT_\tau\rho_\tau)$$
$$-\gamma(\xi)(AV_TT_{\tau\tau\tau}+3AV_{TT}T_\tau T_{\tau\tau}+AV_{TTT}T_\tau{}^3-3AV_TT_\tau\rho_\tau{}^2-3AV\rho_{\tau\tau}\rho_\tau)+\mu(\xi,\tau)AV$$
$$+\alpha_3(\xi)A^2|V|^2AV_TT_\tau+\eta(\xi)AV\rho_\tau\pm\sigma(\xi,\tau)AT_\tau V_T=0, \quad (4)$$

where the scripts of differential equations are simplified as $A(\xi)=A$, $Z(\xi)=Z$, $T(\xi,\tau)=T$, $\rho(\xi,\tau)=\rho$, and $V[Z(\xi),T(\xi,\tau)]=V$. According to the previous works [55,59], we use the symmetry reduction given by Eq. (2) that would reduce Eq. (1) to the higher-order integrable Hirota equation in the form [60]

$$i\frac{\partial V}{\partial Z}=-\frac{\partial^2V}{\partial T^2}+G|V|^2V+2\sqrt{2}i\nu\left(\frac{\partial^3V}{\partial T^3}+3|V|^2\frac{\partial V}{\partial T}\right). \quad (5)$$

In the case of rogue waves finding, we take $G=-1$ to obtain rational solutions. The parameter ν is a real constant. With $V[Z(\xi),T(\xi,\tau)]$ satisfying the relation Eq. (5), the similarity reduction of Eqs. (3) and (4) yields

$$\gamma(\xi)T_\tau T_{\tau\tau}=0, \quad (6)$$

$$T_\xi+2d(\xi)T_\tau\rho_\tau+2P(\xi,\tau)T_\tau\rho_\tau\pm\sigma(\xi,\tau)T_\tau-\gamma(\xi)(T_{\tau\tau\tau}-3T_\tau\rho_\tau{}^2)=0, \quad (7)$$

$$A_\xi+A[d(\xi)\rho_{\xi\xi}+\rho_{\tau\tau}P(\xi,\tau)+3\gamma(\xi)\rho_{\tau\tau}\rho_\tau+\mu(\xi,\tau)+\eta(\xi)\rho_\tau]=0, \quad (8)$$

$$\gamma(\xi)T_\tau{}^3+2\sqrt{2}\nu Z_\xi=0, \quad (9)$$

$$A_\xi V+AZ_\xi V_Z+AT_\xi V_T=0, \quad (10)$$

$$\alpha_3(\xi)A^2T_\tau-6\sqrt{2}\nu Z_\xi=0, \quad (11)$$

$$d(\xi)T_{\xi\xi}+P(\xi,\tau)T_{\tau\tau}+3\gamma(\xi)(T_{\tau\tau}\rho_\tau+T_\tau\rho_{\tau\tau})+\eta(\xi)T_\tau=0, \quad (12)$$

$$Z_\xi+d(\xi)T_\xi{}^2+P(\xi,\tau)T_\tau{}^2+3\gamma(\xi)\rho_\tau T_\tau{}^2=0, \quad (13)$$

$$\rho_\xi+d(\xi)\rho_\xi{}^2+P(\xi,\tau)\rho_\tau{}^2+\gamma(\xi)(\rho_\tau{}^3-\rho_{\tau\tau\tau})\pm\sigma(\xi,\tau)\rho_\tau\pm D(\xi,\tau)=0, \quad (14)$$

$$GZ_\xi+A^2(C(\xi,\tau)+\alpha_3(\xi)\rho_\tau)=0, \quad (15)$$

$$A_{\xi\xi}V+2A_\xi Z_\xi V_Z+2A_\xi T_\xi V_T+2AZ_\xi T_\xi V_{ZT}+AZ_{\xi\xi}V_Z+AZ_\xi{}^2V_{ZZ}=0. \quad (16)$$

Here, the subscripts ξ and τ denote spatial and temporal derivatives, respectively. Through the above symmetry reduction method, the constraints or integrability conditions of the model given in Eq. (1) are derived from the differential equations of which the simplified forms stand from Eq. (6) to Eq. (16), respectively, as follows $-3AV_{TT}\neq0$, $AV_T\neq0$, $V\neq0$, $-AV_{TTT}\neq0$, $2d\rho_\xi\neq0$, $A|V|^2V_T\neq0$, $AV_T\neq0$, $AV_{TT}\neq0$, $-AV\neq0$, $-A|V|^2V\neq0$, and $d\neq0$.

We should keep in mind that each constraint plays an important role in the choice of arbitrary functions and parameters of the system. To have an aperture of dynamics behavior of parameters, the above equations should be solved to give the information on the form and order of each coefficient of the model and on variables related to the complex field. The resolution of Eq. (6) yields for $\gamma(\xi)\neq0$ and for $T_\tau T_{\tau\tau}=0$ to the similarity variable

$$T(\xi,\tau)=T_1(\xi)\tau+T_0(\xi), \quad (17)$$

where $T_1(\xi)$ and $T_0(\xi)$ are arbitrary functions. From Eq. (9), the effective propagation distance $Z(\xi)$ will be

$$Z(\xi)=-\frac{\sqrt{2}}{4\nu}\int_0^\xi\gamma(s)T_1(s)^3ds. \quad (18)$$

Equation (11) gives the result

$$\alpha_3(\xi)=-3\gamma(\xi)T_1{}^2(\xi)A^{-2}(\xi). \quad (19)$$

$\alpha_3(\xi)$ has the physical sense of SS. The substitution of Eq. (17) into Eq. (12) tends to $d(\xi)T_{\xi\xi}+3\gamma(\xi)T_\tau\rho_{\tau\tau}+\eta(\xi)T_\tau=0$. As $\gamma(\xi)\neq0$, $T_1(\xi)\neq0$, and $T_{\xi\xi}=T_{1_{\xi\xi}}\tau+T_{0_{\xi\xi}}$, the phase of the envelope field can be written as

$$\rho(\xi,\tau)=\rho_3(\xi)\tau^3+\rho_2(\xi)\tau^2+\rho_1(\xi)\tau+\rho_0(\xi), \quad (20)$$

with

$$\rho_3(\xi)=-\frac{1}{18}\frac{d(\xi)T_1(\xi)_{\xi\xi}}{\gamma(\xi)T_1(\xi)},$$
$$\rho_2(\xi)=-\frac{1}{6}\frac{d(\xi)T_0(\xi)_{\xi\xi}+\eta(\xi)T_1(\xi)}{\gamma(\xi)T_1(\xi)}, \quad (21)$$

where $\rho_1(\xi)$ and $\rho_0(\xi)$ are arbitrary functions. Through relation Eq. (15), one finds that

$$C(\xi,\tau)=C_2(\xi)\tau^2+C_1(\xi)\tau+C_0(\xi), \quad (22)$$

with

$$C_2(\xi) = -\frac{1}{2}\frac{T_1(\xi)d(\xi)T_1(\xi)_{\xi\xi}}{A(\xi)^2},$$
$$C_1(\xi) = -\frac{T_1(\xi)[d(\xi)T_0(\xi)_{\xi\xi} + T_1(\xi)^2\eta(\xi)]}{A(\xi)^2}, \quad (23)$$
$$C_0(\xi) = \frac{\gamma(\xi)\,T_1(\xi)^2}{A(\xi)^2}\left[3\,\rho_1(\xi) + \frac{1}{4}\frac{\sqrt{2}GT_1(\xi)}{\nu}\right].$$

$C(\xi,\tau)$ is the space- and time-modulated SPM. Equation (13) stands for

$$P(\xi,\tau) = P_2(\xi)\tau^2 + P_1(\xi)\tau + P_0(\xi), \quad (24)$$

with

$$P_2(\xi) = \frac{1}{2}\frac{d(\xi)T_1(\xi)_{\xi\xi}}{T_1(\xi)} - \frac{d(\xi)T_1(\xi)_\xi{}^2}{T_1(\xi)^2},$$
$$P_1(\xi) = \eta(\xi) + \frac{d(\xi)T_0(\xi)_{\xi\xi}}{T_1(\xi)} - 2\frac{d(\xi)T_1(\xi)_\xi T_0(\xi)_\xi}{T_1(\xi)^2}, \quad (25)$$
$$P_0(\xi) = \frac{1}{4}\frac{\gamma(\xi)\,T_1(\xi)\sqrt{2}}{\nu} - 3\,\gamma(\xi)\,\rho_1(\xi) - \frac{d(\xi)T_0(\xi)_\xi{}^2}{T_1(\xi)^2}.$$

$P(\xi,\tau)$ is the space- and time-modulated GVD. Through Eq. (7), we arrive at

$$\pm\sigma(\xi,\tau) = \sigma_4(\xi)\tau^4 + \sigma_3(\xi)\tau^3 + \sigma_2(\xi)\tau^2 + \sigma_1(\xi)\tau + \sigma_0(\xi), \quad (26)$$

where the parameters $\sigma_4(\xi)$, $\sigma_3(\xi)$, $\sigma_2(\xi)$, $\sigma_1(\xi)$, and $\sigma_0(\xi)$ are expressed in Appendix B. $\pm\sigma(\xi,\tau)$ is the left- and right-hand side of the walk-off effect. Equation instead of relation Eq. (8) is transformed to

$$A(\xi) = A_0\exp\left\{\int_0^\xi f(s)ds\right\}, \quad (27)$$

where A_0 is a constant and with

$$f = \mu_3(\xi)\tau^3 + \mu_2(\xi)\tau^2 + \mu_1(\xi)\tau + \mu_0(\xi) - \mu(\xi,\tau),$$
$$\mu(\xi,\tau) = \mu_3(\xi)\tau^3 + \mu_2(\xi)\tau^2 + \mu_1(\xi)\tau + 2\mu_0(\xi), \quad (28)$$

where the parameters of the gain or loss term $\mu(\xi,\tau)$ are given in Appendix C. $\mu(\xi,\tau)$ is the space- and time-modulated gain or loss term. It follows from the above equations that the amplitude of the envelope field becomes

$$A(\xi) = A_0\exp\left\{\int_0^\xi -\mu_0(s)ds\right\}, \quad (29)$$

with

$$\mu_0(\xi) = -\frac{1}{3}\frac{d(\xi)T_0(\xi)_\xi{}^2\eta(\xi)}{\gamma(\xi)T_1(\xi)^2} - \frac{1}{3}\frac{d(\xi)^2T_0(\xi)_\xi{}^2T_0(\xi)_{\xi\xi}}{\gamma(\xi)T_1(\xi)^3}$$
$$+\frac{1}{12}\frac{T_1(\xi)\sqrt{2}\eta(\xi)}{\nu} - \eta(\xi)\rho_1(\xi)$$
$$+\frac{1}{12}\frac{\sqrt{2}d(\xi)T_0(\xi)_{\xi\xi}}{\nu} - d(\xi)\rho_0(\xi)_{\xi\xi}. \quad (30)$$

The result coming from Eq. (14) is

$$\pm D(\xi,\tau) = D_6(\xi)\tau^6 + D_5(\xi)\tau^5 + D_4(\xi)\tau^4 + D_3(\xi)\tau^3$$
$$+ D_2(\xi)\tau^2 + D_1(\xi)\tau + D_0(\xi), \quad (31)$$

with $D_-(\xi) = -D_+(\xi)$ and where $D_6(\xi)$, $D_5(\xi)$, $D_4(\xi)$, $D_3(\xi)$, $D_2(\xi)$, $D_1(\xi)$, and $D_0(\xi)$ are given in Appendix D. $\pm D(\xi,\tau)$ is the left- and right-hand side of the space- and time-modulated linear birefringence.

The resolution of the above differential equations reveals and confirms the assumption of the space- and time-modulated variable of the TOD, gain or loss term, linear birefringence, SPM, and walk-off coefficients. More specifically, it reveals the optically active nature of the system through the left- and right-hand sides of mathematical expressions of the linear birefringence and walk-off term. In fact, the chirality, known as optical activity in optics, is the ability to rotate plane polarized light and this happens when the plane polarized light hits an optically active compound. The more compounds it hits, the more it rotates. Physically, when the polarized light leaves the chiral optical fiber which is optically active, we have to rotate the analyzer to allow the plane of light to pass through. This angle of rotation, called observed rotation, can be directed to the right-hand side, that is a positive rotation or clockwise rotation, also called dextrorotatory. In the case of which the analyzer has to be rotated to the left-hand side for the polarized light to pass through, that is a negative rotation or counterclockwise rotation, called levorotatory. Hence, the mathematical expressions of relation Eqs. (26) and (31) with positive signs refer to the dextrorotatory components and the ones with negative signs to the levorotatory components of the system. As we can see, they are equal in magnitude but opposite in sign.

We can observe through the above variable coefficients of the model that $P(\xi,\tau)$, $\mu(\xi,\tau)$, $D(\xi,\tau)$, $C(\xi,\tau)$, and $\sigma_3(\xi,\tau)$ are polynomials in τ with coefficients being functions of ξ. Parameters $d(\xi)$, $\gamma(\xi)$, $\alpha_3(\xi)$, and $\eta(\xi)$ are arbitrary functions, except the SS, which depends on the TOD and amplitude. Since the nonparaxial parameter $d(\xi)$, the differential gain or loss term $\eta(\xi)$, and third-order dispersion $\gamma(\xi)$ are major functions of the base equation coefficients, it appears from analytical results that they are are the main keys to control the amplitude, the SS, the GVD, the SPM, the walk-off term, and linear birefringence in optical fibers. Therefore, they can be considered as specific control parameters of the system. The TOD coefficient $\gamma(\xi)$ can also be used to control the effective propagation distance $Z(\xi)$. The gain or loss term of the induce optical activity $\mu(\xi,\tau)$ can be used to manage the optical activity on the amplitude $A(\xi)$, SS coefficient $\alpha_3(\xi)$, and on the SPM nonlinearity $C(\xi,\tau)$.

According to the MDT method [47–49,61], which is well-known and clearly derived by many authors, the first- and second-order of the complex field $V[Z(\xi),T(\xi,\tau)]$ are expressed by Akhmediev *et al.* [60]. It is good to mention that the first-order of the complex field $V[Z(\xi),T(\xi,\tau)]$ was found by Peregrine [40] and the second-order by Akhmediev *et al.* [62]. Later, Ankiewicz *et al.* [60] found the first- and second-order of the Hirota equation. By considering the correspondence $Z(\xi) = x$, $\frac{1}{\sqrt{2}}T(\xi,\tau) = t$, and $\nu = \alpha_3$, in this last reference,

the first-order complex field $V[Z(\xi),T(\xi,\tau)]$ yields

$$V_1[Z(\xi),T(\xi,\tau)] = \left[1 - \frac{G_1 + iH_1}{D_1}\right] \exp\{iZ(\xi)\}, \quad (32)$$

where

$$\begin{aligned} &G_1 = 4, \quad H_1 = 8Z(\xi), \\ &D_1 = 1 + [\sqrt{2}T(\xi,\tau) + 12\nu Z(\xi)]^2 + 4Z(\xi)^2. \end{aligned} \quad (33)$$

The partial solution Eq. (32), is known as the Peregrine soliton [40]. Then, collecting this solution together with the founded amplitude and phase of the wave, we construct the first-order rational solution related to the nonparaxial chiral optical rogue wave given by

$$\psi_1 = A(\xi)\left[1 - \frac{G_1 + iH_1}{D_1}\right] \exp\{iZ(\xi) + i\rho(\xi,\tau)\}, \quad (34)$$

which result becomes

$$\begin{aligned} \psi_1 = A_0 \exp\left\{-\int_0^{\xi} \mu_0(s)ds\right\} \\ \times \left[1 - \frac{G_1 + iH_1}{D_1}\right] \exp\{iZ(\xi) + i\rho(\xi,\tau)\}. \end{aligned} \quad (35)$$

This first-order rational solution is used to describe the propagation of nonparaxial optical rogue wave in a fiber filled with chiral materials. For suitable choice of arbitrary parameters of the original Eq. (1), we can manage through a simultaneous controllability, the rogue wave structures with the specific control parameters. The second-order rational solution of the complex field $V[Z(\xi),T(\xi,\tau)]$ stands for

$$V_2[Z(\xi),T(\xi,\tau)] = \left[1 + \frac{G_2 + iZ(\xi)H_2}{D_2}\right] \exp i\{Z(\xi)\}, \quad (36)$$

where G_2, H_2, and D_2 are given by the relations

$$\begin{aligned} G_2 = &-48T^4 - 1152\sqrt{2}\nu ZT^3 - 144T^2[4Z^2(36\nu^2+1)+1] \\ &- 576\sqrt{2}\nu ZT[12Z^2(12\nu^2+1)+7] - 192Z^4 \\ &\times [216(6\nu^4+\nu^2)+5] - 864Z^2(44\nu^2+1) - 36, \\ H_2 = &-96T^4 - 2304\sqrt{2}\nu ZT^3 - 96T^2[4Z^2(108\nu^2+1)-3] \\ &- 1152\sqrt{2}\nu ZT[4Z^2(36\nu^2+1)] - 384Z^4(36\nu^2+1)^2 \\ &- 192Z^2(180\nu^2+1) + 360, \\ D_2 = &\, 8T^6 + 288\sqrt{2}\nu ZT^5 - 432Z^4(624\nu^4 - 40\nu^2 - 1) \\ &+ 36Z^2(556\nu^2+11) + 9 + 64Z^6(36\nu^2+1)^3 + 96\sqrt{2} \\ &\times ZT^3[12Z^2(60\nu^2+1) - 1] \\ &+ 12T^4[4Z^2(180\nu^2+1)+1] \\ &+ 6T^2[16Z^4[216\nu^2(30\nu^2+1) - 1] \\ &- 24Z^2(60\nu^2+1) + 9] + 72\sqrt{2}\nu ZT[16Z^4(36\nu^2+1) \\ &+ 8Z^2(1 - 108\nu^2) + 17]. \end{aligned} \quad (37)$$

According to the same correspondence joined with the founded variables including the above solutions, the second-order rational solution, related to a particular solution of Eq. (1), was obtained:

$$\psi_2 = A(\xi)\left[1 + \frac{G_2 + iZ(\xi)H_2}{D_2}\right] \exp\{iZ(\xi) + i\rho(\xi,\tau)\}. \quad (38)$$

Then, the construction of the second-order nonparaxial chiral optical rogue wave yields

$$\begin{aligned} \psi_2 = A_0 \exp\left\{-\int_0^{\xi} \mu_0(s)ds\right\} \\ \times \left[1 + \frac{G_2 + iZ(\xi)H_2}{D_2}\right] \exp\{iZ(\xi) + i\rho(\xi,\tau)\}. \end{aligned} \quad (39)$$

These second-order rational solutions arise due to the collision between two or more ultrashort pulses in the optical fiber. More specifically, they are nonparaxial chiral optical rogue waves which can propagate through a fiber filled with chiral materials. The particularity of these solutions is the simultaneous controllability of their amplitudes through the three specific control parameters, which can be used to manage the intensity and the shape of the waves. As the nonparaxiality, TOD, and differential gain or loss terms depend on specific control parameterts, they can therefore provide a more convenient and controlled environment to experimentally study specific optical communication problems.

III. DYNAMICS BEHAVIOR AND FEATURES OF COMBINED EFFECT ON NONPARAXIAL CHIRAL OPTICAL ROGUE WAVES

After the construction of the above solutions, the parameters are chosen to investigate the dynamics behavior and the features of combined effects on nonparaxial chiral optical rogue waves. Afterwards, we plot the specific control parameters of the system, the GVD, and the amplitudes of the envelope field in the left- and right-hand sides to have an aperture of their dynamic in the nonparaxial chiral optical fiber (see Figs. 1, 2, and 3).

Then, we alternate the sign of chiral parameters in both space and time in the first and second order of nonparaxial

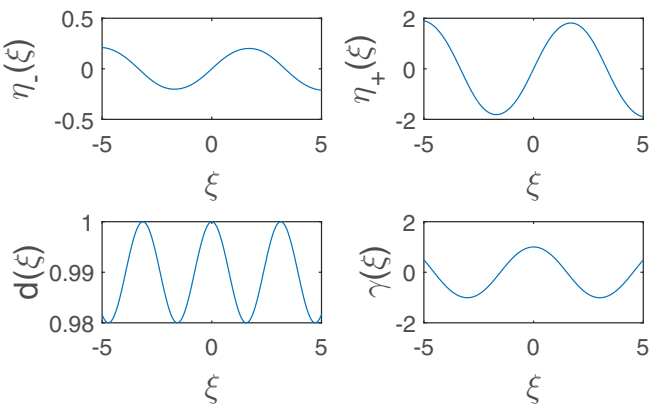

FIG. 1. Specific control parameters: the left- and right-hand side of the gain or loss differential term $\eta(\xi)$, nonparaxial parameter $d(\xi)$, and TOD $\gamma(\xi)$, where $\eta(\xi) = C_T sn(\xi,k_7)$, $d(\xi) = dn(\xi,k_5)$, $\gamma(\xi) = cn(\xi,k_6)$, and $C_T = 1 \pm KT_c$, with $k_5 = 0.2$, $k_6 = 0.4$, $k_7 = 0.5$, and $KT_c = 0.8$.

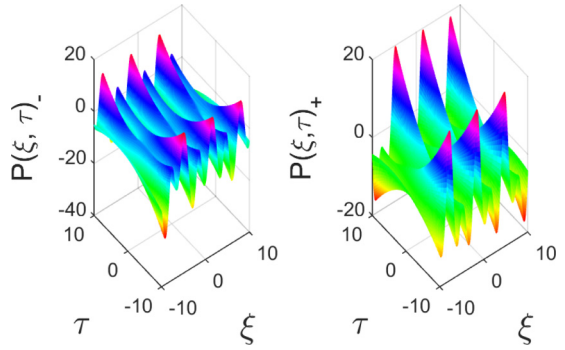

FIG. 2. The space- and time-modulated group velocity dispersion $P(\xi,\tau)$ on the left- and right-hand side, respectively, expressed in relation Eq. (24), where $\eta(\xi) = C_T sn(\xi,k_7)$, $d(\xi) = dn(\xi,k_5)$, $\gamma(\xi) = cn(\xi,k_6)$, $T_0(\xi) = sn(\xi,k_3)$, $T_1(\xi) = dn(\xi,k_3)$, $\rho_0(\xi) = dn(\xi,k_2)$, $\rho_1(\xi) = cn(\xi,k_1)$, and $C_T = 1 \pm KT_c$, with $k_1 = 0.3$, $k_2 = 0.5$, $k_3 = 0.6$, $k_4 = 0.4$, $k_5 = 0.2$, $k_6 = 0.4$, $k_7 = 0.5$, $\nu = 0.2$, and $KT_c = 0.8$.

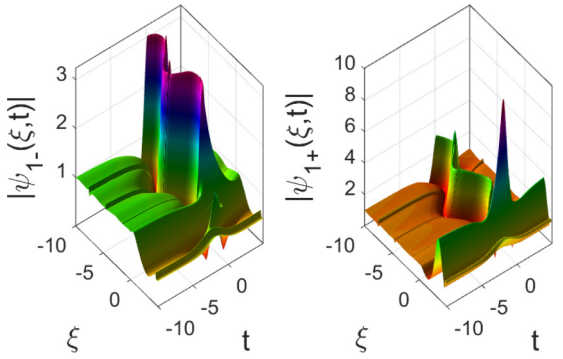

FIG. 4. First-order nonparaxial chiral optical rogue waves on the left- and right-hand side of the rational solution given by Eq. (35), where $\eta(\xi) = C_T sn(\xi,k_7)$, $d(\xi) = dn(\xi,k_5)$, $\gamma(\xi) = cn(\xi,k_6)$, $T_0(\xi) = sn(\xi,k_3)$, $T_1(\xi) = dn(\xi,k_3)$, $\rho_0(\xi) = dn(\xi,k_2)$, $\rho_1(\xi) = cn(\xi,k_1)$, and $C_T = 1 \pm KT_c$, with $k_1 = 0.3$, $k_2 = 0.5$, $k_3 = 0.6$, $k_4 = 0.4$, $k_5 = 0.2$, $k_6 = 0.4$, $k_7 = 0.5$, $\nu = 0.2$, and $KT_c = 0.8$.

chiral optical rogue wave solutions to analyze their behavior and therefore to optimize the eventual stability of the solutions (see Figs. 4 and 5).

Figure 1 depicts the dynamical behavior of each specific parameter in the system. On the one hand, we can observe the influence of chiral nature of the differential gain or loss term through its weak peak in the left-hand side and high peak in the right-hand side. On the other hand, the amplitude and the width of each parameter depend on the value of their moduli $k_i (i = 5,6,7)$ and on the type of Jacobian elliptic function they carry (cn,dn,sn). The left- and right-hand sides of the space- and time-modulated group-velocity dispersion $P(\xi,\tau)$ are illustrated in Fig. 2 and expressed by relation Eq. (24) with their arbitrary Jacobian elliptic functions and moduli given in the figure caption. It can be seen that the structure of GVD differs from one side to the other. Figure 3 depicts the profiles of the amplitudes of the envelope field $A(\xi)$ on both sides. We remark on the trace of each evolution, the presence of two dark-bright collisions in the right-hand side and two bright-dark collisions in the left-hand side. These collisions are better observed through analytical simulation of the first- and second-order nonparaxial chiral optical rogue waves which are illustrated in Figs. 4 and 5. Throughout these figures, we notice a main difference on the structure and on the amplitude of the first- and second-order in both sides. We also remark an energy transfer from the left-hand to right-hand side on each solution.

More specifically, in Fig. 3 we can see the contrast of optical activity in the sense of oscillation of each component of the amplitude as it increase then decrease on the left-hand side, whereas it decreases then increases on the right-hand side. Generally, in optically active media, components are equal in magnitude but different in sign. However, in this case, the equality of magnitude is affected by the differential gain or loss term $\eta(\xi) = (1 \pm KT_c) sn(\xi,k_7)$, which is responsible for the observed difference on both sides and, consequently, on both sides of the amplitude. It can be seen throughout Fig. 1 that the amplitude of the differential gain or loss term is four times higher in the right-hand side compare to the left-hand side. Now, when we look at the mathematical expression of the space- and time-modulated GVD, we denote that it depends also on the differential gain or loss term; however, GVD profiles are nearly equal in magnitude, as shown in Fig. 2. This

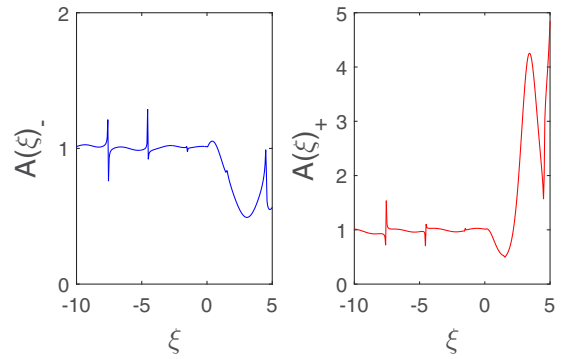

FIG. 3. The left- and right-hand side amplitude $A(\xi)$, presented in relation Eq. (29), where $\eta(\xi) = C_T sn(\xi,k_7)$, $d(\xi) = dn(\xi,k_5)$, $\gamma(\xi) = cn(\xi,k_6)$, $T_0(\xi) = sn(\xi,k_3)$, $T_1(\xi) = dn(\xi,k_3)$, $\rho_0(\xi) = dn(\xi,k_2)$, $\rho_1(\xi) = cn(\xi,k_1)$, and $C_T = 1 \pm KT_c$, with $k_1 = 0.3$, $k_2 = 0.5$, $k_3 = 0.6$, $k_4 = 0.4$, $k_5 = 0.2$, $k_6 = 0.4$, $k_7 = 0.5$, and $KT_c = 0.8$.

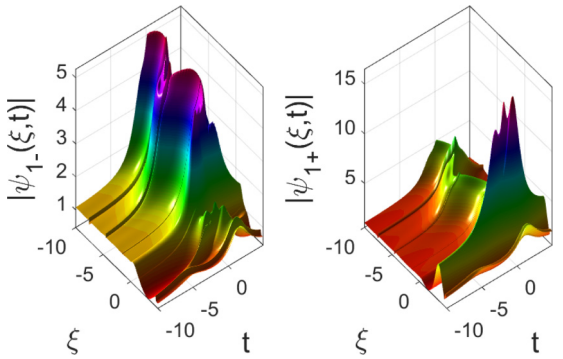

FIG. 5. Second-order nonparaxial chiral optical rogue waves on the left- and right-hand side of the rational solution given by Eq. (39), where $\eta(\xi) = C_T sn(\xi,k_7)$, $d(\xi) = dn(\xi,k_5)$, $\gamma(\xi) = cn(\xi,k_6)$, $T_0(\xi) = sn(\xi,k_3)$, $T_1(\xi) = dn(\xi,k_3)$, $\rho_0(\xi) = dn(\xi,k_2)$, $\rho_1(\xi) = cn(\xi,k_1)$, and $C_T = 1 \pm KT_c$, with $k_1 = 0.3$, $k_2 = 0.5$, $k_3 = 0.6$, $k_4 = 0.4$, $k_5 = 0.2$, $k_6 = 0.4$, $k_7 = 0.5$, $\nu = 0.2$, and $KT_c = 0.8$.

contrast is due to the fact that the differential gain or loss term plays a role of loss in the expression of the amplitude and the role of gain in the expression of GVD. This is an advantage for the waves, which become more stable as we can see in Figs. 4 and 5. As the vector NLS equations describe extreme waves with higher accuracy than the scalar NLS equation models, we are going to use the vector nonparaxial NLS equations to enrich the work.

IV. THE INFLUENCE OF COMBINED EFFECTS ON THE NUMERICAL SOLUTIONS OF VECTOR NONPARAXIAL NLS EQUATIONS WITH CONSTANT COEFFICIENTS

To illustrate the nonparaxiality, optical activity, and walk-off effects on the propagation of nonparaxial chiral optical rogue waves, we derive from the model obtained in Eq. (A25) the vector nonparaxial NLS equations with constant and modulated coefficients which governs the propagation of rogons in optical fibers filled with chiral materials. So doing, the coupled system of the nonparaxial NLS equation with constant coefficients is given by

$$\begin{aligned} &d\psi_{1\xi\xi} + i\psi_{1\xi} + P\psi_{1\tau\tau} - i\gamma\psi_{1\tau\tau\tau} + i\mu\psi_1 \mp D\psi_1 - C(|\psi_1|^2 + |\psi_2|^2)\psi_1 + i\alpha_3(|\psi_1|^2 + |\psi_2|^2)\psi_{1\tau} + (\eta \pm i\sigma)\psi_{1\tau} = 0,\\ &d\psi_{2\xi\xi} + i\psi_{2\xi} + P\psi_{2\tau\tau} - i\gamma\psi_{2\tau\tau\tau} + i\mu\psi_2 \mp D\psi_2 - C(|\psi_1|^2 + |\psi_2|^2)\psi_2 + i\alpha_3(|\psi_1|^2 + |\psi_2|^2)\psi_{2\tau} + (\eta \pm i\sigma)\psi_{2\tau} = 0. \end{aligned} \tag{40}$$

To simplify the expressions of waves functions, we let $\psi_1(\xi,\tau) = u(\xi,\tau)$ and $\psi_2(\xi,\tau) = v(\xi,\tau)$. In this part of the work, we focus our attention on the generation and propagation of bright and dark rogue wave solutions when the nonparaxial effect arises fundamentally from chiral optical fibers. To study the influence of combined effects of the nonparaxiality, optical activity, and walk-off on optical rogue wave propagation, we used an algorithm scheme derived by Chamorro-Posada *et al.* [37], namely, difference-differential equation method that has a wider applicability on nonparaxial beam propagation methods. In this method, we used the finite difference formulas to approximate derivatives with respect to ξ coordinate, and then the fast Fourier transforms (FFTs) are used to compute efficiently the second- and third-order diffractions in the spectral domain.

The finite difference formulas for the derivatives are given in Appendix E. Substituting these formulas in the coupled nonparaxial NLS equations with constant coefficients, we obtained the difference-differential equations below:

$$\begin{aligned} u_{n+1}(\tau) = \frac{1}{2d + i\Delta\xi}\Bigg[\Bigg(&4d - 2P\Delta\xi^2\frac{\partial^2}{\partial\tau^2} + 2i\gamma\Delta\xi^2\frac{\partial^3}{\partial\tau^3} - 2i\mu\Delta\xi^2 \pm 2\Delta\xi^2 D + 2C\Delta\xi^2(|u_n(\tau)|^2 + |v_n(\tau)|^2)\\ &- 2i\alpha_3\Delta\xi^2(|u_n(\tau)|^2 + |v_n(\tau)|^2)\frac{\partial}{\partial\tau} - 2\Delta\xi^2(\eta \pm i\sigma)\frac{\partial}{\partial\tau}\Bigg)u_n(\tau) - (2d - i\Delta\xi)u_{n-1}(\tau)\Bigg],\\ v_{n+1}(\tau) = \frac{1}{2d + i\Delta\xi}\Bigg[\Bigg(&4d - 2P\Delta\xi^2\frac{\partial^2}{\partial\tau^2} + 2i\gamma\Delta\xi^2\frac{\partial^3}{\partial\tau^3} - 2i\mu\Delta\xi^2 \pm 2\Delta\xi^2 D + 2C\Delta\xi^2(|u_n(\tau)|^2 + |v_n(\tau)|^2)\\ &- 2i\alpha_3\Delta\xi^2(|u_n(\tau)|^2 + |v_n(\tau)|^2)\frac{\partial}{\partial\tau} - 2\Delta\xi^2(\eta \pm i\sigma)\frac{\partial}{\partial\tau}\Bigg)v_n(\tau) - (2d - i\Delta\xi)v_{n-1}(\tau)\Bigg]. \end{aligned} \tag{41}$$

These equations define the explicit algorithm in which the effects of the transverse differential operators $\frac{\partial^2}{\partial\tau^2}$ and $\frac{\partial^3}{\partial\tau^3}$ are computed efficiently and accurately by the FFTs. An implementation on the index n gives us the numerical solutions of each component. We used as initial conditions, the rational solutions of the envelope fields [30], constructed by the DDT method, where we consider the correspondence $t \to \xi$ and $x \to \tau$:

$$\begin{aligned} u(\xi,\tau) &= u_{01}\left(\frac{p^2\tau^2 + p^4\xi^2 + p\tau(\alpha_1 + \beta\theta_1) - i\alpha_1 p^2\xi + \beta\theta_1}{p^2\tau^2 + p^4\xi^2 + \beta(p\tau + 1)}\right)\\ v(\xi,\tau) &= v_{01}\left(\frac{p^2\tau^2 + p^4\xi^2 + p\tau(\alpha_2 + \beta\theta_2) - i\alpha_2 p^2\xi + \beta\theta_2}{p^2\tau^2 + p^4\xi^2 + \beta(p\tau + 1)}\right), \end{aligned} \tag{42}$$

where the parameters are

$$\begin{aligned} &u_{01} = a_1\exp[i(q_1\tau - v_1\xi)] \quad v_{01} = a_1\exp[i(q_2\tau - v_2\xi)],\\ &v_1 = q_1^2 + 2\left(a_1^2 + a_2^2\right) \quad v_2 = {q_2}^2 + 2\left(a_1^2 + a_2^2\right),\\ &\alpha_1 = \frac{4p^2}{p^2 + 4{q_1}^2} \quad \alpha_2 = \frac{4p^2}{p^2 + 4{q_2}^2},\\ &\theta_1 = \frac{2q_1 + ip}{2q_1 - ip} \quad \theta_2 = \frac{2q_2 + ip}{2q_2 - ip}, \end{aligned} \tag{43}$$

with

$$\begin{aligned} &p = 2\mathrm{Im}(\lambda + k), \quad \chi = \mathrm{Im}(k), \quad q_1 + q_2 = 2\mathrm{Re}(\lambda + k),\\ &q_1 - q_2 = 2q, \quad \beta = \frac{p^3}{\chi(p^2 + 4q_1q_2)},\\ &k = 2.36954 + 1.1972i,\\ &\lambda = -1.69162 - 1.79721i. \end{aligned} \tag{44}$$

To plot the numerical solutions, we choose appropriately, free functions $T_1(\xi)$, $T_0(\xi)$, $\mu(\xi)$, and $\gamma(\xi)$ and the Jacobian elliptic

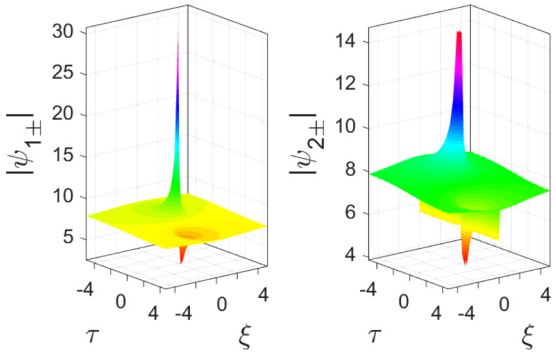

FIG. 6. Nonparaxial chiral optical vector rogue waves with constant coefficients on the right- and left-hand side $|\psi_{1,2}(\xi,\tau)|$, where the parameters are $a_1 = 3, a_2 = 3, d = 10, P = -0.5, \gamma = 0.4, \mu = 0.3, D = \pm 0.6, C = 2, \alpha 3 = 0.2, \eta = 0.5, \sigma = \pm 0.1, k_1 = 0.3, k_2 = 0.5, k_3 = 0.6, k_4 = 0.4, k_5 = 0.2, k_6 = 0.4,$ and $k_7 = 0.5$. Here, the initial conditions take the form of exact solution Eqs. (42), (43), and (44).

functions below [64]:

$$dn(z,k) = 1 - \frac{k^2 \sin(z)^2}{2},$$
$$cn(z,k) = \cos(z) - k^2 \sin(z)\left[\frac{z - \sin(z)\cos(z)}{4}\right], \quad (45)$$
$$sn(z,k) = \sin(z) - k^2 \cos(z)\left[\frac{z - \sin(z)\cos(z)}{4}\right].$$

The parameters are chosen to be bounded in the intervals $-10 < \xi < 10$ and $-10 < \tau < 10$. Curves are plotted with the help of Matlab through a pseudospectral method. So doing, we obtained identical right- and left-hand sides of nonparaxial chiral optical vector rogue waves with constant coefficients (see Figs. 6, 7, and 8).

These representations showed us the rapid convergence of the pseudospectral method based on the difference-differential equation method [37] when $\Delta\xi/d \to 0$. In the case of constant coefficients, it can be seen that the vector nonparaxial

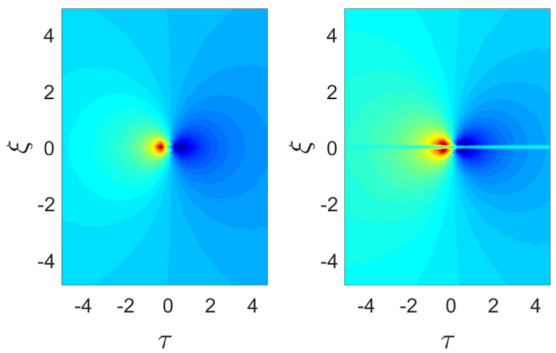

FIG. 7. Two-dimensional representations of the nonparaxial chiral optical vector rogue waves with constant coefficients in both sides, where the initial conditions take the form of exact solution Eqs. (42), (43), and (44) with the following parameters: $a_1 = 1, a_2 = 1, d = 100, P = -0.5, \gamma = 0.4, \mu = 0.3, D = \pm 0.6, C = 2, \alpha 3 = 0.2, \eta = 0.5, \sigma = \pm 0.1, k_1 = 0.3, k_2 = 0.5, k_3 = 0.6, k_4 = 0.4, k_5 = 0.2, k_6 = 0.4,$ and $k_7 = 0.5$.

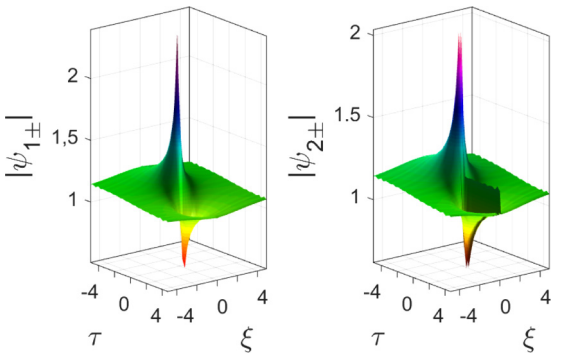

FIG. 8. Nonparaxial chiral optical vector rogue waves with constant coefficients in both sides, where the initial conditions are expressed in the form of exact solutions Eqs. (42), (43), and (44) with the parameters $a_1 = 1, a_2 = 1, d = 10, P = -0.5, \gamma = 0.4, \mu = 0.3, D = \pm 0.6, C = 2, \alpha 3 = 0.2, \eta = 10, \sigma = \pm 10, k_1 = 0.3, k_2 = 0.5, k_3 = 0.6, k_4 = 0.4, k_5 = 0.2, k_6 = 0.4,$ and $k_7 = 0.5$.

chiral optical rogue waves are localized in space and time as usual rogue waves and that the forward and backward of each component are similar. We notice that the mixture of bright and dark structures on each component are due to

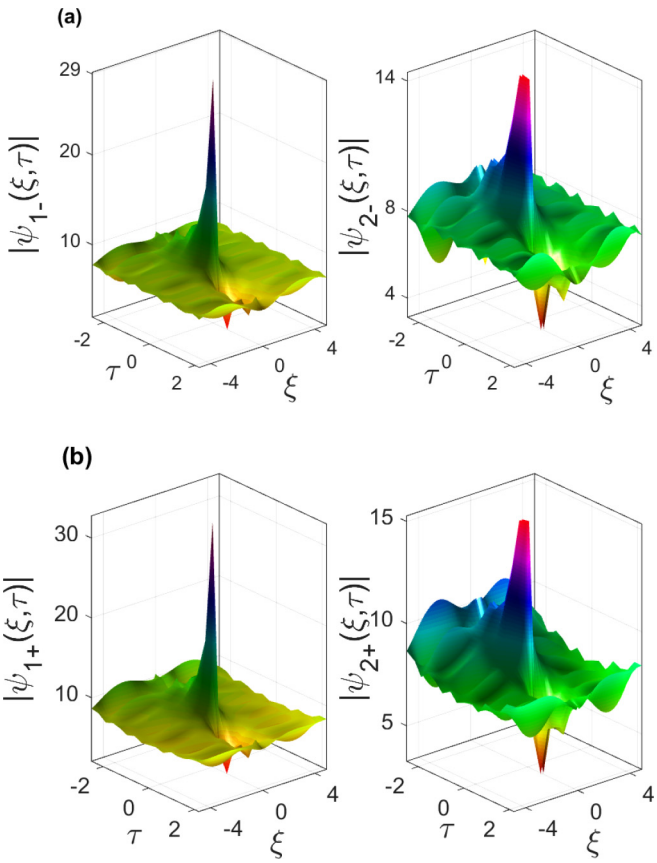

FIG. 9. The nonparaxial chiral optical rogue waves with management are derived from Eqs. (49), where the parameters of the base equations are given in relation Eqs. (47) and (46) and the initial conditions take the form of exact solutions given in relation Eqs. 42, 43, and 44, with the following arbitrary constants: $a_1 = 3, a_2 = 3, k_5 = 0.2, k_6 = 0.4, k_7 = 0.5, P(\xi,\tau) = dn(\xi,k)\tau^2 + cn(\xi,k)\tau + sn(\xi,k)$, $KT_c = 0.8$, and $C_T = 1 \pm KT_c$.

the coupling of vectorial model on the one hand, and to the interaction between waves as consequence of narrowness of the two components in the system on the other hand. The two-dimensional representations of Fig. 7 showed the limit of the extension of bright and dark spectral structures in the retarded time axis at $\tau = 0$. We can see how the intensity of each spectrum increases when $\tau \to 0$ and the attenuation when we are moving from each side of $\tau = 0$. We noted that the weak values of the walk-off are responsible for the wave smoothing.

V. INFLUENCE OF COMBINED EFFECTS ON THE VECTOR NONPARAXIAL CHIRAL NLS EQUATIONS WITH MODULATED COEFFICIENTS

To improve the description of the waves, we use the vector nonparaxial chiral NLS equations with modulated coefficients. From the model obtained in Eq. (A25), the coupled system of the nonparaxial NLS equations in chiral optical fibers with coupled space-dependence coupling field is expressed as

$$\begin{aligned}
&d(\xi)\psi_{1\xi\xi} + i\psi_{1\xi} + P(\xi,\tau)\psi_{1\tau\tau} - i\gamma(\xi)\psi_{1\tau\tau\tau} + i\mu(\xi,\tau)\psi_1 \\
&\quad \mp D(\xi,\tau)\psi_1 - C(\xi,\tau)(|\psi_1|^2 + |\psi_2|^2)\psi_1 + i\alpha_3(\xi) \\
&\qquad \times (|\psi_1|^2 + |\psi_2|^2)\psi_{1\tau} + [\eta(\xi) \pm i\sigma(\xi,\tau)]\psi_{1\tau} = 0, \\
&d(\xi)\psi_{2\xi\xi} + i\psi_{2\xi} + P(\xi,\tau)\psi_{2\tau\tau} - i\gamma(\xi)\psi_{2\tau\tau\tau} + i\mu(\xi,\tau)\psi_2 \\
&\quad \mp D(\xi,\tau)\psi_2 - C(\xi,\tau)(|\psi_1|^2 + |\psi_2|^2)\psi_2 + i\alpha_3(\xi) \\
&\qquad \times (|\psi_1|^2 + |\psi_2|^2)\psi_{2\tau} + [\eta(\xi) \pm i\sigma(\xi,\tau)]\psi_{2\tau} = 0. \quad (46)
\end{aligned}$$

It can been seen from Eqs. (2) that the differential gain and loss term $\eta(\xi)$, the self-steepening $\alpha_3(\xi)$, the gain or loss term $\mu(\xi,\tau)$, and the self-phase modulation $C(\xi,\tau)$ depend on chiral parameter T_c through the relation $C_T = 1 \pm KT_c$ and the linear birefringence $D(\xi,\tau)$ and walk-off term $\sigma(\xi,\tau)$ are functions of chiral parameter T_c. Considering the order of polynomials of each parameter of the number like Eq. (1) obtained from the analytical results, we can choose them as Jacobian elliptic functions for the good stability of the waves and their forms, arbitrarily

$$\begin{aligned}
\alpha_3(\xi) &= C_T \times cn(\xi,k), \;\; \eta(\xi) = C_T \times sn(\xi,k), \\
d(\xi) &= dn(\xi,k), \;\; \gamma(\xi) = cn(\xi,k), \\
C(\xi,\tau) &= [dn(\xi,k)\tau^2 + cn(\xi,k)\tau + sn(\xi,k)] \times C_T, \\
P(\xi,\tau) &= -[dn(\xi,k)\tau^2 + cn(\xi,k)\tau + sn(\xi,k)], \\
\mu(\xi,\tau) &= [dn(\xi,k)\tau^3 + cn(\xi,k)\tau^2 + sn(\xi,k)\tau + dn(\xi,k)] \times C_T, \\
\sigma(\xi,\tau) &= [dn(\xi,k)\tau^4 + cn(\xi,k)\tau^3 + sn(\xi,k)\tau^2 + dn(\xi,k)\tau + cn(\xi,k)] \times KT_c, \\
D(\xi,\tau) &= [dn(\xi,k)\tau^6 + cn(\xi,k)\tau^5 + sn(\xi,k)\tau^4 + dn(\xi,k)\tau^3 + cn(\xi,k)\tau^2 + sn(\xi,k)\tau + dn(\xi,k)]KT_c. \quad (47)
\end{aligned}$$

One may also choose them as polynomial functions but our interest is motivated by functions that can generate stable waves. As the propagation variable ξ tends to $n\Delta\xi$ in the discretized domain, the Jacobian elliptic functions take the form

$$\begin{aligned}
dn(\xi,k) &\to dn(n\Delta\xi,k) = 1 - \frac{k^2 \sin(n\Delta\xi)^2}{2}, \\
cn(\xi,k) &\to cn(n\Delta\xi,k) = \cos(n\Delta\xi) - k^2 \sin(n\Delta\xi)\left\{\frac{n\Delta\xi - \sin[n\Delta\xi\cos(n\Delta\xi)]}{4}\right\}, \quad (48) \\
sn(\xi,k) &\to sn(n\Delta\xi,k) = \sin(n\Delta\xi) - k^2 \cos(n\Delta\xi)\left\{\frac{n\Delta\xi - \sin[n\Delta\xi\cos(n\Delta\xi)]}{4}\right\}.
\end{aligned}$$

It can be seen that, by splitting Eqs. (46) in the right- and left-hand sides, we obtained four coupled nonparaxial NLS equations which differ by the signs of linear birefringence and walk-off term. The substitution of the finite difference formulas in Eqs. (46) yields

$$\begin{aligned}
u_{n+1}(\tau) = \frac{1}{2d(n\Delta\xi) + i\Delta\xi}\Bigg[\Bigg(&4d(n\Delta\xi) - 2P(n\Delta\xi,\tau)\Delta\xi^2\frac{\partial^2}{\partial\tau^2} + 2i\gamma(n\Delta\xi)\Delta\xi^2\frac{\partial^3}{\partial\tau^3} - 2i\mu(n\Delta\xi,\tau)\Delta\xi^2 \pm 2\Delta\xi^2 D(n\Delta\xi,\tau) \\
&+ 2C(n\Delta\xi,\tau)\Delta\xi^2(|u_n(\tau)|^2 + |v_n(\tau)|^2) - 2i\alpha_3(n\Delta\xi)\Delta\xi^2(|u_n(\tau)|^2 + |v_n(\tau)|^2)\frac{\partial}{\partial\tau} \\
&- 2\Delta\xi^2(\eta(n\Delta\xi) \pm i\sigma(n\Delta\xi,\tau))\frac{\partial}{\partial\tau}\Bigg)u_n(\tau) - (2d(n\Delta\xi,\tau) - i\Delta\xi)u_{n-1}(\tau)\Bigg], \\
v_{n+1}(\tau) = \frac{1}{2d(n\Delta\xi) + i\Delta\xi}\Bigg[\Bigg(&4d(n\Delta\xi) - 2P(n\Delta\xi,\tau)\Delta\xi^2\frac{\partial^2}{\partial\tau^2} + 2i\gamma(n\Delta\xi)\Delta\xi^2\frac{\partial^3}{\partial\tau^3} - 2i\mu(n\Delta\xi,\tau)\Delta\xi^2 \pm 2\Delta\xi^2 D(n\Delta\xi,\tau) \\
&+ 2C(n\Delta\xi,\tau)\Delta\xi^2(|u_n(\tau)|^2 + |v_n(\tau)|^2) - 2i\alpha_3(n\Delta\xi)\Delta\xi^2(|u_n(\tau)|^2 + |v_n(\tau)|^2)\frac{\partial}{\partial\tau} \\
&- 2\Delta\xi^2(\eta(n\Delta\xi) \pm i\sigma(n\Delta\xi,\tau))\frac{\partial}{\partial\tau}\Bigg)v_n(\tau) - (2d(n\Delta\xi,\tau) - i\Delta\xi)v_{n-1}(\tau)\Bigg]. \quad (49)
\end{aligned}$$

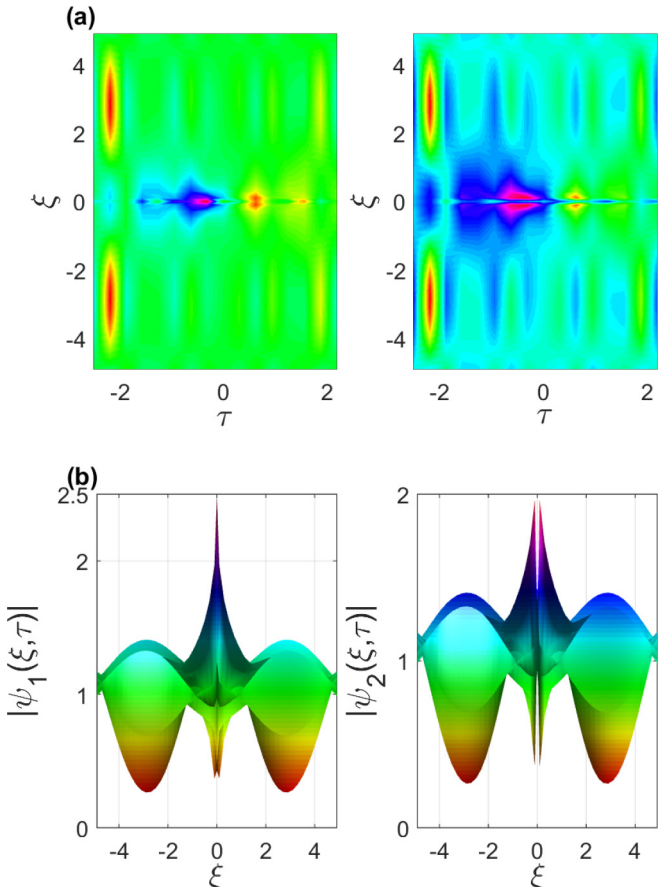

FIG. 10. The two-dimensional representation of the nonparaxial chiral optical vector rogue waves with variable coefficients are derived from Eqs. (49), where the parameters of the base equations are given in relation Eqs. (47) and (46) and the initial conditions take the form of exact solutions given in relation Eqs. (42), (43) and (44), with the following arbitrary constants: $a_1 = 1, a_2 = 1, k_5 = 0.2, k_6 = 0.4, k_7 = 0.5$, $P(\xi,\tau) = dn(\xi,k)\tau^2 + cn(\xi,k)\tau + sn(\xi,k)$, $KT_c = 0.8$, and $C_T = 1 \pm KT_c$.

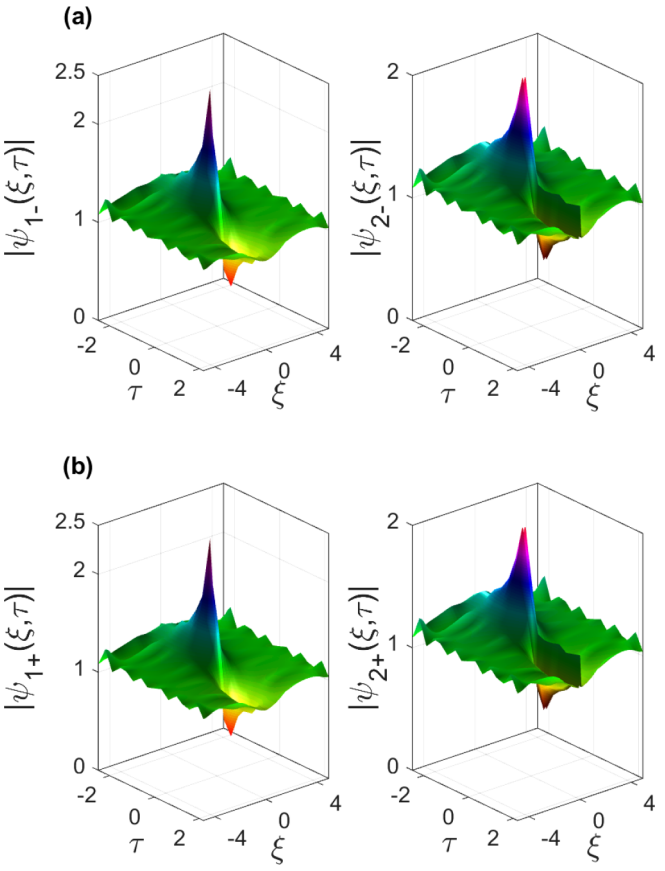

FIG. 11. Nonparaxial chiral optical vector rogue waves with modulated coefficients are derived from Eqs. (49) where the parameters of the base equations are given in relations Eqs. (47) and (46) and where the initial conditions take the form of exact solutions given in relations Eqs. (42), (43), and (44), with the following arbitrary constants: $a_1 = 1, a_2 = 1$ and $k_5 = k_6 = k_7 = 1, d(\xi) = 10 \times dn(\xi,k)$, $P(\xi,\tau) = -(dn(\xi,k)\tau^2 + cn(\xi,k)\tau + sn(\xi,k))$, $KT_c = 0.8$, and $C_T = 1 \pm KT_c$.

By using the difference-differential equation method and fast Fourier transforms (FFTs), we plot the numerical solutions of the coupled nonparaxial chiral NLS equations of each beam (ψ_1 and ψ_2) in both sides, left ($-$) and right ($+$) (see Figs. 9–11).

Throughout these figures, we remark that the structure of each component is similar from one hand to the other but a notable difference is observed in the amplitude as we can see in Fig. 9. The two-dimensional representations depict in Fig. 10(a), the symmetries of the bright and dark maxima through the retarded time axis τ and the dark-dark symmetries through the propagation distance axis ξ in both side. On Fig. 10(b), we can observe a significant decrease of the envelope fields when we reduce the amplitudes of the seeding solutions. We also denote a similitude on the structure and amplitude in Figs. 11. The appearance of curvatures in the four components are due to the unity value of their moduli as expressed in Fig. 11.

VI. CONCLUSION

We derived both scalar and vector nonparaxial NLS equations with constant and modulated coefficients to improve the description of rogue waves propagation in optical fibers filled with chiral materials. Our models, in particular, verified the assumption of controllability on the one hand, and takes into account the parameters responsible for the nonparaxiality, optical activity, and walk-off effect, on the other hand. The first- and second-order nonparaxial chiral optical rogue waves were investigated by the MDT method. As the nonparaxiality, TOD, and differential gain or loss terms depend on specific control parameters $d(\xi)$, $\gamma(\xi)$, and $\eta(\xi)$, it appeared that they are the main keys to control the amplitude of the envelope fields, SS, GVD, SPM, walk-off effect, linear birefringence, and the effective propagation distance. Therefore, we have concluded that among previous models that have been studied before, the models derived in this work allowed us to improve the description of rogue waves and their control in chiral optical fibers with higher-order nonlinear effects. In these models, we also denoted the influences of TOD and differential gain or loss term. Then, the algorithm scheme derived for the nonparaxial beam propagation methods, namely, difference-differential equation method, was used to compute efficiently the diffractions in the spectral domain. After many numerical

simulation tests, we remarked that the increase or decrease of the three specific control parameters can affect the wave shape and the amplitude of each component. We have also shown that, among those specific control parameters, the nonparaxial coefficient has the most influential effect, whereas the two others that are differential gain or loss and walk-off terms are physically inactive. We found that in the absence of nonparaxial parameter, the influence of the two others are effective and equivalent. We also noticed that in the absence of two specific control parameters, the last one becomes the powerful influential effect in the system.

We improved our understanding through models under consideration of combined effects on rogue wave propagation in optical fibers filled with chiral materials. We have shown the necessity to take into account the parameters responsible of the simultaneous controllability of different effects in the system. Those parameters revealed the control key and the novel properties of nonparaxial chiral optical rogue wave solutions. For specific parameter values, usual rogue waves, such as the vector Peregrine, were obtained, showing the collisions between bright and dark rogue waves. The study of combined effects has allowed us to determine the powerful influence among the effects, and the nonparaxial effect was claimed to be the most influential one. The vector rogue wave solutions based on the vector nonparaxial NLS equations, which modeled the coupling of two nonlinear waves under the assumptions of nonparaxiality, optical activity, and walk-off, contributed to better control rogue wave phenomena in optical fibers filled with chiral materials and in a variety of complex dynamics.

ACKNOWLEDGMENTS

This work was supported by the Organization for Women in Science for the Developing World (OWSD) and Swedish International Development Cooperation Agency (Sida) under Grant No. 3240287309. We are also grateful to University of the Western Cape for research facilities and computer services.

APPENDIX A: THE DERIVATION OF THE HOMOGENEOUS HIGHER-ORDER NONPARAXIAL NLS IN CHIRAL OPTICAL FIBERS

We consider a model that satisfies both the breakdown of the paraxial approximation as well as the requirements of time-reversal symmetry and reciprocity through the Drude-Born-Federov formalism. Under this formalism, the adequate constitutive relations for the study of propagation of waves in chiral medium are expressed as [63–65]

$$\vec{D} = \varepsilon_n \vec{E} + \varepsilon_0 T_c \vec{\nabla} \times \vec{E}, \quad \vec{B} = \mu_0 (\vec{H} + T_c \vec{\nabla} \times \vec{H}), \tag{A1}$$

where the flux densities $\vec{D}$ and $\vec{B}$ arise in response to the electric and magnetic field $\vec{E}$ and $\vec{H}$ propagating in the chiral medium with $\varepsilon_n = \varepsilon_0 + \varepsilon_2 |\vec{E}|^2$. Here, ε_0 and ε_2 are linear and nonlinear permittivity, respectively. μ_0 is the permeability and T_c the chiral parameter of the optical fiber. In the chiral optical medium, the predicted Maxwell equations can be written as

$$\begin{aligned} &\vec{\nabla} \cdot \vec{D} = \rho_v, \quad \vec{\nabla} \cdot \vec{B} = 0, \\ &\vec{\nabla} \times \vec{E} = -\frac{\partial \vec{B}}{\partial t}, \quad \vec{\nabla} \times \vec{H} = \vec{J} + \frac{\partial \vec{D}}{\partial t}, \end{aligned} \tag{A2}$$

where the current density $\vec{J} = \sigma \vec{E}$ and the charge density ρ represents the sources for the electromagnetic field. The quantity σ is the electrical conductivity and v is the volume. Substituting Eq. (A1) into Eq. (A2), we obtain the following wave equation:

$$\begin{aligned} &\nabla^2 \vec{E} + \mu_0 \varepsilon T^2 \frac{\partial^2 \vec{\nabla}^2 \vec{E}}{\partial t^2} \\ &= \mu_0 \varepsilon_0 \frac{\partial^2 \vec{E}}{\partial t^2} + \mu_0 \sigma \frac{\partial \vec{E}}{\partial t} + \mu_0 \varepsilon_2 |\vec{E}|^2 \frac{\partial^2 \vec{E}}{\partial t^2} \\ &\quad + 2\mu_0 \varepsilon_0 T \vec{\nabla} \times \frac{\partial^2 \vec{E}}{\partial t^2} + \mu_0 \varepsilon_2 T |\vec{E}|^2 \vec{\nabla} \times \frac{\partial^2 \vec{E}}{\partial t^2} \\ &\quad + \mu_0 \sigma T \vec{\nabla} \times \frac{\partial \vec{E}}{\partial t}. \end{aligned} \tag{A3}$$

The optical field $\vec{E}$ is represented by right-hand (R) or left-hand (L) polarizations in the z direction as

$$\begin{aligned} \vec{E}(\vec{r},t) &= (\hat{x} \mp j\hat{y}) A(\vec{r},t) \exp[-j(k_{\pm} z - \omega_0 t)] \\ &= \vec{\psi}_{R,L} \exp[-j(k_{\pm} z - \omega_0 t)], \end{aligned} \tag{A4}$$

where $\vec{\psi}_{R,L}$ is the complex envelope of the optical field in the nonlinear chiral medium, K is the wave number, and ω_0 is the frequency.

After evaluation of different derivations of $\vec{E}$ in x, y, and z directions in Eq. (A3), we neglect all the second-order terms, except the nonparaxial one. Considering that the wave is propagating in the z direction implies

$$K_x = K_y = 0, \quad E_z = 0. \tag{A5}$$

Therefore, Eq. (A3) is reduced in x, y, and z directions, respectively, as follows:

$$\begin{aligned} &\left(1 - \mu_0 \varepsilon_0 T_c^2 \omega^2\right)\left[\frac{\partial^2 E_x}{\partial x^2} + \frac{\partial^2 E_x}{\partial y^2} + \frac{\partial^2 E_x}{\partial z^2}\right] - 2jK_z \frac{\partial E_x}{\partial z} - K_z^2 E_x \\ &\quad + \mu_0 \varepsilon T_c^2 \left(\omega^2 K_z^2 E_x + 2jK_z \omega^2 \frac{\partial E_x}{\partial z} - 2jK_z^2 \omega \frac{\partial E_x}{\partial t} - K_z^2 \frac{\partial^2 E_x}{\partial t^2}\right) \\ &= (\mu_0 \varepsilon_0 + \mu_0 \varepsilon_2 |\vec{E}|^2)\left[\frac{\partial^2 E_x}{\partial t^2} + 2j\omega \frac{\partial E_x}{\partial t} - \omega^2 E_x\right] + \mu_0 \sigma \left(\frac{\partial E_x}{\partial t} + j\omega E_x\right) \\ &\quad + (2\mu_0 \varepsilon_0 T_c + \mu_0 \varepsilon_2 T_c |\vec{E}|^2)\left[\omega^2 \frac{\partial E_y}{\partial z} + jK_z \left(\frac{\partial^2 E_y}{\partial t^2} + 2j\omega \frac{\partial E_y}{\partial t} - \omega^2 E_y\right)\right] + \mu_0 \sigma T_c \left(-j\omega \frac{\partial E_y}{\partial z} + jK_z \frac{\partial E_y}{\partial t} - \omega K_z E_y\right), \end{aligned} \tag{A6}$$

$$\begin{aligned}
&\left(1-\mu_0\varepsilon_0T_c^2\omega^2\right)\left[\frac{\partial^2E_y}{\partial x^2}+\frac{\partial^2E_y}{\partial y^2}+\frac{\partial^2E_y}{\partial z^2}\right]-2jK_z\frac{\partial E_y}{\partial z}-K_z^2E_y\\
&\quad+\mu_0\varepsilon T_c^2\left(\omega^2K_z^2E_y+2jK_z\omega^2\frac{\partial E_y}{\partial z}-2jK_z^2\omega\frac{\partial E_y}{\partial t}-K_z^2\frac{\partial^2E_y}{\partial t^2}\right)\\
&=(\mu_0\varepsilon_0+\mu_0\varepsilon_2|\vec{E}|^2)\left[\frac{\partial^2E_y}{\partial t^2}+2j\omega\frac{\partial E_y}{\partial t}-\omega^2E_y\right]+\mu_0\sigma\left(\frac{\partial E_y}{\partial t}+j\omega E_y\right)+(2\mu_0\varepsilon_0T+\mu_0\varepsilon_2T|\vec{E}|^2)\\
&\quad\times\left[-\omega^2\frac{\partial E_x}{\partial z}-jK_z\left(\frac{\partial^2E_x}{\partial t^2}+2j\omega\frac{\partial E_x}{\partial t}-\omega^2E_x\right)\right]+\mu_0\sigma T(j\omega\frac{\partial E_x}{\partial z}-jK_z\frac{\partial E_x}{\partial t}+\omega K_zE_x),
\end{aligned}\tag{A7}$$

$$[-(2\mu_0\varepsilon_0T_c+\mu_0\varepsilon_2T_c|\vec{E}|^2)\omega^2+j\omega\mu_0\sigma T_c]\left[\frac{\partial E_y}{\partial x}-\frac{\partial E_x}{\partial y}\right]=0.\tag{A8}$$

Equation (A8) leads to

$$\frac{\partial E_y}{\partial x}=\frac{\partial E_x}{\partial y}=cst,\quad E_y=E_y(z,t),\quad E_x=E_x(z,t).\tag{A9}$$

We multiply Eq. (A7) by $\pm j$, and we do the addition of Eqs. (A6) and (A7), where we consider the conditions given in relation Eq. (A9) and the following approximations:

$$\left|\frac{\partial E_x}{\partial t}\right|\ll|2j\omega E_x|,\quad\left|\frac{\partial^2E_y}{\partial z^2}\right|\ll|2j\omega E_y|.\tag{A10}$$

Therefore, the alternative form of the wave equation can be written as

$$\begin{aligned}
&\left(1-\mu_0\varepsilon_0T_c^2\omega^2\right)\frac{\partial^2\psi_{R,L}}{\partial z^2}+\{-2jK_z+2jK_z\omega^2\mu_0\varepsilon T_c^2\pm j[(2\mu_0\varepsilon_0T_c+\mu_0\varepsilon_2T_c|\vec{E}|^2)\omega^2-j\omega\mu_0\sigma T_c]\}\frac{\partial\psi_{R,L}}{\partial z}\\
&+\{-K_z^2+\mu_0\varepsilon_0T_c^2\omega^2K_z^2+\omega^2(\mu_0\varepsilon_0+\mu_0\varepsilon_2|\vec{E}|^2)-j\omega\mu_0\sigma\pm j[-jK_z\omega^2(2\mu_0\varepsilon_0T_c+\mu_0\varepsilon_2T_c|\vec{E}|^2)\\
&-K_z\omega\mu_0\sigma T_c]\}\psi_{R,L}+\{-2jK_z^2\omega\mu_0\varepsilon_0T_c^2-\mu_0\sigma-2j\omega(\mu_0\varepsilon_0+\mu_0\varepsilon_2|\vec{E}|^2)\pm j[-2\omega K_z(2\mu_0\varepsilon_0T_c\\
&+\mu_0\varepsilon_2T_c|\vec{E}|^2)+jK_z\mu_0\sigma T_c]\}\frac{\partial\psi_{R,L}}{\partial t}=0,
\end{aligned}\tag{A11}$$

where $\psi_{R,L}=E_x\pm jE_y$. Then, the reference changing is

$$\begin{aligned}
&\psi_R=E_x+jE_y\quad\psi_L=E_x-jE_y,\\
&E_x=\frac{\psi_R+\psi_L}{2}\quad E_y=\frac{\psi_R-\psi_L}{2}.
\end{aligned}\tag{A12}$$

The division of Eq. (A6) by $-2K_z$ yields

$$\begin{aligned}
&-\frac{\left(1-\mu_0\varepsilon_0T_c^2\omega^2\right)}{2K_z}\frac{\partial^2\psi_{R,L}}{\partial z^2}+j\left(1-K_0^2T_c^2\right)\frac{\partial\psi_{R,L}}{\partial z}\mp j\frac{K_0^2T_c}{K_z}\frac{\partial\psi_{R,L}}{\partial z}+j\frac{\omega\mu_0\varepsilon_2}{K_z}|\psi_{R,L}|^2\frac{\partial\psi_{R,L}}{\partial t}\mp j\frac{\mu_0\varepsilon_2\omega^2T_c}{2K_z}\\
&\times|\psi_{R,L}|^2\frac{\partial\psi_{R,L}}{\partial z}+j\frac{K_0}{K_zc}\left(1+K_z^2T_c^2\right)\frac{\partial\psi_{R,L}}{\partial t}\pm\frac{j\omega\mu_0\sigma T_c}{2}\psi_{R,L}+\frac{1}{2}\left(K_z-K_zK_0^2T_c^2-\frac{K_0^2}{K_z}\right)\psi_{R,L}\\
&-\frac{\mu_0\varepsilon_2\omega^2}{2K_z}|\psi_{R,L}|^2\psi_{R,L}\mp\frac{\omega^2}{2}\left(\mu_0\varepsilon_2T_c|\psi_{R,L}|^2\right)\psi_{R,L}+j\frac{\omega\mu_0\sigma}{2K_z}\psi_{R,L}\mp K_0^2T_c\psi_{R,L}\mp\frac{\omega\mu_0\sigma T}{2K_z}\frac{\partial\psi_{R,L}}{\partial z}\\
&\pm\frac{\mu_0\sigma T_c}{2}\frac{\partial\psi_{R,L}}{\partial t}\pm j\frac{2K_0T_c}{C}\frac{\partial\psi_{R,L}}{\partial t}+\frac{\mu_0\sigma}{2K_z}\frac{\partial\psi_{R,L}}{\partial t}\pm j\omega\mu_0\varepsilon_2T_c|\psi_{R,L}|^2\frac{\partial\psi_{R,L}}{\partial t}=0,
\end{aligned}\tag{A13}$$

where

$$K_0=\frac{\omega}{c},\quad\mu_0\varepsilon_0c^2=1.\tag{A14}$$

The dispersion relation is given by

$$K_z=\frac{K_0}{1\pm K_0T_c}.\tag{A15}$$

For $K_0^2 T_c^2 \ll 1$, we get $K_z = K_0$. By neglecting the nonlinear diffraction, the second and the last terms of Eq. (A13), and for the following set of parameters become

$$v^2 = \frac{1}{\mu_0 \varepsilon_0}, \quad \alpha = \mu_0 \sigma, \quad \beta = \mu_0 \varepsilon_2, \quad K_0 = \frac{\omega}{v}, \quad z^* = \frac{z}{1 - K_0^2 T_c^2}. \tag{A16}$$

Equation (A13) takes the form

$$-\frac{1}{2K_0}\frac{\partial^2 \psi_{R,L}}{\partial z^{*2}} + j\frac{\partial \psi_{R,L}}{\partial z^*} + j\frac{1}{v}\frac{\partial \psi_{R,L}}{\partial t} + j\frac{\omega\alpha}{2K_0}(1 \pm K_0 T_c)\psi_{R,L} \mp K_0^2 T_c \psi_{R,L} - \frac{\beta\omega^2}{2K_0}(1 \pm K_0 T_c)$$
$$\times |\psi_{R,L}|^2 \psi_{R,L} + \frac{\alpha}{2K_0}(1 \pm K_0 T_c)\frac{\partial \psi_{R,L}}{\partial t} \pm \frac{j2K_0^2 T_c}{\omega}\frac{\partial \psi_{R,L}}{\partial t} + \frac{j\omega\beta}{K_0}(1 \pm K_0 T_c)|\psi_{R,L}|^2 \frac{\partial \psi_{R,L}}{\partial t} = 0. \tag{A17}$$

If we let

$$\psi_{R,L} = \phi, \text{ then } K = K_0 = K_z. \tag{A18}$$

Equation (A16) yields

$$-\frac{1}{2K}\frac{\partial^2 \phi}{\partial z^{*2}} + j\frac{\partial \phi}{\partial z^*} + j\frac{1}{v}\frac{\partial \phi}{\partial t} + j\frac{\omega\alpha}{2K}(1 \mp K T_c)\phi - \frac{\beta\omega^2}{2K}(1 \mp K T_c)|\phi|^2\phi \mp K^2 T_c \phi$$
$$+\frac{\alpha}{2K}(1 \pm K T_c)\frac{\partial \phi}{\partial t} \pm j\frac{2K^2 T_c}{\omega}\frac{\partial \psi_{R,L}}{\partial t} + j\frac{\omega\beta}{K_0}(1 \pm K T_c)|\phi|^2\frac{\partial \phi}{\partial t} = 0. \tag{A19}$$

The Taylor series of the wave number $K(\omega)$ at the third-order and the Fourier transform of $\Delta\omega$ and ΔK help to express in an approximate form, the second term of Eq. (A18) as

$$j\frac{1}{v}\frac{\partial \phi}{\partial t} = j\frac{1}{v_g}\frac{\partial \phi}{\partial t} + \frac{1}{2}K''\frac{\partial^2 \phi}{\partial t^2} - j\frac{1}{6}K'''\frac{\partial^3 \phi}{\partial t^3}, \tag{A20}$$

where

$$K'' = \frac{\partial^2 K}{\partial \omega^2}, K''' = \frac{\partial^3 K}{\partial \omega^3}, K' = \frac{1}{v_g} = \frac{\partial K}{\partial \omega}. \tag{A21}$$

Then, for the following change of variable:

$$\begin{aligned} t' &= t - \frac{1}{v_g}z^* \\ z' &= z^*, \end{aligned} \Rightarrow \begin{aligned} \frac{\partial}{\partial t} &\to \frac{\partial}{\partial t'} \\ \frac{\partial}{\partial z^*} &\to \frac{\partial}{\partial z'} - \frac{1}{v_g}\frac{\partial}{\partial t'}, \end{aligned} \tag{A22}$$

Eq. (A19) stands for

$$-\frac{1}{2K}\frac{\partial^2 \phi}{\partial z'^2} + j\frac{\partial \phi}{\partial z'} + \frac{1}{2}\left(K'' - \frac{K'^2}{K}\right)\frac{\partial^2 \phi}{\partial t'^2} - j\frac{1}{6}K'''\frac{\partial^3 \phi}{\partial t'^3} + j\frac{\omega\alpha}{2K}(1 \pm K T_c)\phi - \frac{\beta\omega^2}{2K}(1 \mp K T_c)|\phi|^2\phi \mp K^2 T \phi$$
$$+\frac{\alpha}{2K}(1 \pm K T_c)\frac{\partial \phi}{\partial t'} \pm j\frac{2K^2 T_c}{\omega}\frac{\partial \phi}{\partial t'} + j\frac{\omega\beta}{K}|\phi|^2(1 \pm K T_c)\frac{\partial \phi}{\partial t'} = 0, \tag{A23}$$

where $K' = \frac{\partial K}{\partial \omega} = \frac{1}{v_g}$ is the inverse of group-velocity, $K'' = \frac{\partial K'}{\partial \omega}$ is the group-velocity dispersion (GVD) coefficient, which can take the plus and minus signs ($\pm$), representing the anomalous and normal dispersion regimes, respectively. The parameter $K''' = \frac{\partial K''}{\partial \omega}$ is the third-order dispersion (TOD) term. In the fourth term, the attenuation coefficient α is weighted toward the chiral parameter T_c. The factor to $|\phi|^2\phi$ is the self-phase modulation (SPM) and the term $K^2 T_c \phi$ occurs as an additional correction to the chirality of the fiber. The expressions at the eighth and ninth positions are the differential gain or loss term and the walk-off effect. The last term has the physical sense of self-steepening (SS) and is necessary to perform the description of spontaneous waves.

The new variables, namely,

$$q = \frac{{\omega_0}^{2/3}\beta^{1/3}}{(2K_0)^{1/3}}\phi, \quad \xi = \frac{{\omega_0}^{2/3}\beta^{1/3}}{(2K_0)^{1/3}}z', \quad d = -\frac{\beta^{1/3}{\omega_0}^{2/3}}{(2k_0)^{4/3}},$$
$$\eta = \frac{\alpha C_T}{\sqrt{K''}{\omega_0}^{1/3}\beta^{1/6}(2k_0)^{5/6}}, \quad \tau = \frac{{\omega_0}^{1/3}\beta^{1/16}}{\sqrt{K''}(2K_0)^{1/6}}t',$$
$$\gamma = \frac{K'''}{6}\frac{\beta^{1/6}{\omega_0}^{1/3}}{(2K_0)^{1/6}(K'')^{3/2}}, \quad C_T = 1 \mp T_c K,$$

$$\Gamma = \frac{{\omega_0}^{1/3}\alpha}{(2K_0)^{1/3}\beta^{1/3}}, \quad \mu = C_T\Gamma, \quad P = \frac{1}{2}\left(1 - \frac{k'^2}{K''k_0}\right),$$
$$\sigma_3 = \frac{k_0 T_c (2k_0)^{7/6}}{\sqrt{K''}{\omega_0}^{4/3}\beta^{1/6}}, \quad D = \frac{K^2 T_c (2K_0)^{1/3}}{\beta^{1/3}{\omega_0}^{2/3}},$$
$$\alpha_3 = \frac{C_T(2K_0)^{5/6}\beta^{1/6}}{\sqrt{K''}{\omega_0}^{2/3}K_0}, \tag{A24}$$

allow us to express for $q(\xi,\tau) = \psi(\xi,\tau)$, and Eq. (A23) in the form

$$d\frac{\partial^2\psi}{\partial\xi^2} + j\frac{\partial\psi}{\partial\xi} + P\frac{\partial^2\psi}{\partial\tau^2} - j\gamma\frac{\partial^3\psi}{\partial\tau^3} + j\mu\psi \mp D\psi - C_T|\psi|^2\psi + j\alpha_3|\psi|^2\frac{\partial\psi}{\partial\tau} + \eta\frac{\partial\psi}{\partial\tau} \pm j\sigma_3\frac{\partial\psi}{\partial\tau} = 0. \tag{A25}$$

Equation (A25) is the higher-order nonparaxial chiral NLSE and can be used to describe the propagation of the right-hand (+) and left-hand (−) polarized rogue waves in a higher-order dispersive and nonlinear chiral optical fiber. For $d = 0$, $P = \frac{1}{2}$, $T_c = 0$, $C_T = 1$, $D = 0$, $\gamma = 0$, $\mu = 0$, $\eta = 0$, and $\sigma_3 = 0$, Eq. (A25) stands for the standard NLS equation.

APPENDIX B: THE PARAMETERS OF THE WALK-OFF EFFECT $\sigma(\xi,\tau)$

$$\sigma_4(\xi) = -\frac{1}{3}\frac{d(\xi)^2T_1(\xi)_\xi^2T_1(\xi)_{\xi\xi}}{T_1(\xi)^3\gamma(\xi)} + \frac{1}{12}\frac{d(\xi)^2T_1(\xi)_{\xi\xi}{}^2}{T_1(\xi)^2\gamma(\xi)} - \frac{1}{9}\frac{d(\xi)T_1(\xi)_\xi\left(\frac{d(\xi)T_1(\xi)_{\xi\xi}}{\gamma(\xi)T_1(\xi)}\right)_\xi}{T_1(\xi)}, \tag{B1}$$

$$\sigma_3(\xi) = -\frac{2}{3}\frac{d(\xi)^2T_1(\xi)_\xi{}^2T_0(\xi)_{\xi\xi}}{T_1(\xi)^3\gamma(\xi)} - \frac{2}{3}\frac{d(\xi)^2T_1(\xi)_\xi T_0(\xi)_\xi T_1(\xi)_{\xi\xi}}{T_1(\xi)^3\gamma(\xi)} - \frac{2}{3}\frac{d(\xi)\,T1_z{}^2\eta(\xi)}{T_1(\xi)^2\gamma(\xi)} + \frac{1}{3}\frac{d(\xi)T_1(\xi)_\xi\left(\frac{d(\xi)T_0(\xi)_{\xi\xi}+\eta(\xi)T_1(\xi)}{\gamma(\xi)T_1(\xi)}\right)_\xi}{T_1(\xi)}$$
$$+\frac{1}{3}\frac{d\xi\,T_1(\xi)_{\xi\xi}\eta(\xi)}{\gamma(\xi)T_1(\xi)} + \frac{1}{3}\frac{d(\xi)^2T_1(\xi)_{\xi\xi}T_0(\xi)_{\xi\xi}}{T_1(\xi)^2\gamma(\xi)} + \frac{1}{9}\frac{d(\xi)T_0(\xi)_\xi\left(\frac{d\xi\,T_1(\xi)_{\xi\xi}}{\gamma(\xi)T_1(\xi)}\right)_\xi}{T_1(\xi)}, \tag{B2}$$

$$\sigma_2(\xi) = 2\frac{d(\xi)T1(\xi)_\xi^2\rho_1(\xi)}{T_1(\xi)^2} - 2\frac{d(\xi)T_1(\xi)_\xi\rho_1(\xi)_\xi}{T_1(\xi)} - \frac{d(\xi)T_1(\xi)_{\xi\xi}\rho_1(\xi)}{T_1(\xi)} + \frac{2}{3}\frac{d(\xi)T_0(\xi)_{\xi\xi}\eta(\xi)}{\gamma\,(\xi)\,T_1(\xi)} - \frac{4}{3}\frac{d(\xi)\,T_1(\xi)_\xi^2\eta(\xi)}{T_1(\xi)^2\gamma(\xi)}$$
$$+\frac{1}{3}\frac{\eta(\xi)^2}{\gamma(\xi)} + \frac{1}{3}\frac{d(\xi)T_0(\xi)_\xi\left(\frac{d(\xi)\,T_0(\xi)_{\xi\xi}+\eta(\xi)T_1(\xi)}{\gamma\,(\xi)\,T_1(\xi)}\right)_\xi}{T_1(\xi)} + \frac{1}{3}\frac{d(\xi)^2T_0(\xi)_{\xi\xi}^2}{\gamma\,(\xi)\,T_1(\xi)^2} + \frac{1}{12}\frac{\sqrt{2}d(\xi)T_1(\xi)_{\xi\xi}}{\nu}$$
$$-\frac{4}{3}\frac{d(\xi)^2T_1(\xi)_\xi T_0(\xi)_\xi T_0(\xi)_{\xi\xi}}{T_1(\xi)^3\gamma(\xi)} - \frac{1}{3}\frac{d(\xi)^2T_0(\xi)_\xi^2T_1(\xi)_{\xi\xi}}{T_1(\xi)^3\gamma(\xi)}, \tag{B3}$$

$$\sigma_1(\xi) = -2\,\eta(\xi)\rho_1(\xi) - 2\frac{d(\xi)T_1(\xi)_\xi\rho_0(\xi)_\xi}{T_1(\xi)} - 2\frac{d(\xi)\,T_0(\xi)_{\xi\xi}\rho_1(\xi)}{T_1(\xi)} + \frac{1}{6}\frac{\sqrt{2}T_1(\xi)\eta(\xi)}{\nu} - 2\frac{d(\xi)T_0(\xi)_\xi\rho_1(\xi)_\xi}{T_1(\xi)}$$
$$+4\frac{d(\xi)\,T_1(\xi)_\xi T_0(\xi)_\xi\rho_1(\xi)}{T_1(\xi)^2} - \frac{2}{3}\frac{d(\xi)T_0(\xi)_\xi^2\eta(\xi)}{T_1(\xi)^2\gamma(\xi)} + \frac{1}{6}\frac{\sqrt{2}d(\xi)T_0(\xi)_{\xi\xi}}{\nu} - \frac{2}{3}\frac{d(\xi)^2T_0(\xi)_\xi^2T_0(\xi)_{\xi\xi}}{T_1(\xi)^3\gamma(\xi)} - \frac{T_1(\xi)_\xi}{T_1(\xi)}, \tag{B4}$$

$$\sigma_0(\xi) = -12\frac{\sqrt{2}\gamma(\xi)T_1(\xi)\rho_1(\xi)}{\nu} - \frac{T_0(\xi)_\xi}{T_1(\xi)} + 3\,\gamma(\xi)\rho_1(\xi)^2 + 2\frac{d(\xi)\,T_0(\xi)_\xi^2\rho_1(\xi)}{T_1(\xi)^2} - 2\frac{d(\xi)T_0(\xi)_\xi\rho_0(\xi)_\xi}{T_1(\xi)}. \tag{B5}$$

APPENDIX C: THE PARAMETERS OF THE GAIN OR LOSS TERM $\mu(\xi,\tau)$

$$\mu_3(\xi) = -\frac{1}{3}\frac{d(\xi)^2T_1(\xi)_\xi^2T_1(\xi)_{\xi\xi}}{T_1(\xi)^3\gamma(\xi)} + \frac{1}{18}d(\xi)\left(\frac{d(\xi)T_1(\xi)_{\xi\xi}}{\gamma(\xi)T_1(\xi)}\right)_{\xi\xi}, \tag{C1}$$

$$\mu_2(\xi) = \frac{1}{6}\frac{\eta(\xi)d(\xi)T_1(\xi)_{\xi\xi}}{\gamma(\xi)T_1(\xi)} - \frac{1}{3}\frac{d(\xi)T_1(\xi)_\xi^2\eta(\xi)}{T_1(\xi)^2\gamma(\xi)} - \frac{2}{3}\frac{d(\xi)^2T_1(\xi)_\xi T_0(\xi)_\xi T_1(\xi)_{\xi\xi}}{T_1(\xi)^3\gamma(\xi)} - \frac{1}{3}\frac{d(\xi)^2T_1(\xi)_\xi^2T_0(\xi)_{\xi\xi}}{T_1(\xi)^3\gamma(\xi)}$$
$$+\frac{1}{6}d(\xi)\left(\frac{d(\xi)T_0(\xi)_{\xi\xi}+\eta(\xi)T_1(\xi)}{\gamma(\xi)T_1(\xi)}\right)_{\xi\xi}, \tag{C2}$$

$$\mu_1(\xi) = -\frac{2}{3}\frac{d(\xi)T_1(\xi)_\xi T_0(\xi)_\xi\eta(\xi)}{T_1(\xi)^2\gamma(\xi)} + \frac{1}{3}\frac{\eta(\xi)d(\xi)T_0(\xi)_{\xi\xi}}{\gamma(\xi)T_1(\xi)} + \frac{1}{3}\frac{\eta(\xi)^2}{\gamma(\xi)} - \frac{2}{3}\frac{d(\xi)^2T_1(\xi)_\xi T_0(\xi)_\xi T_0(\xi)_{\xi\xi}}{T_1(\xi)^3\gamma(\xi)}$$
$$-\frac{1}{3}\frac{d(\xi)^2T_0(\xi)_\xi^2T_1(\xi)_{\xi\xi}}{T_1(\xi)^3\gamma(\xi)} + \frac{1}{12}\frac{\sqrt{2}d(\xi)T_1(\xi)_{\xi\xi}}{\nu} - d(\xi)\rho_1(\xi)_{\xi\xi}, \tag{C3}$$

$$\mu_0(\xi) = -\frac{1}{3}\frac{d(\xi)T_0(\xi)_\xi^2\eta(\xi)}{\gamma(\xi)T_1(\xi)^2} - \frac{1}{3}\frac{d(\xi)^2T_0(\xi)_\xi^2T_0(\xi)_{\xi\xi}}{\gamma(\xi)T_1(\xi)^3} + \frac{1}{12}\frac{T_1(\xi)\sqrt{2}\eta(\xi)}{\nu} - \eta(\xi)\rho_1(\xi) + \frac{1}{12}\frac{\sqrt{2}d(\xi)T_0(\xi)_{\xi\xi}}{\nu} - d(\xi)\rho_0(\xi)_{\xi\xi}. \tag{C4}$$

APPENDIX D: THE PARAMETERS OF THE LINEAR BIREFRINGENCE $D(\xi,\tau)$

$$D_6(\xi) = -\frac{d(\xi)^2T_1(\xi)_\xi T_1(\xi)_{\xi\xi}\frac{d(\xi)T_1(\xi)_{\xi\xi}}{\gamma(\xi)T_1(\xi)}_\xi}{54\,\gamma(\xi)T_1(\xi)^2} - \frac{d(\xi)^3T_1(\xi)_{\xi\xi}^3}{216\,\gamma(\xi)^2T_1(\xi)^3} + \frac{1}{36}\frac{d(\xi)^3T_1(\xi)_\xi^2T_1(\xi)_{\xi\xi}^2}{T_1(\xi)^4\gamma(\xi)^2}, \tag{D1}$$

$$\begin{aligned}D_5(\xi) = {}& \frac{1}{9}\frac{d(\xi)^2T_1(\xi)_\xi^2T_1(\xi)_{\xi\xi}\eta(\xi)}{T_1(\xi)^3\gamma(\xi)^2} - \frac{d(\xi)^2T_0(\xi)_\xi T_1(\xi)_{\xi\xi}\left(\frac{d(\xi)T_1(\xi)_{\xi\xi}}{\gamma(\xi)T_1(\xi)}\right)_\xi}{54\,\gamma(\xi)T_1(\xi)^2}\\ & -\frac{1}{18}\frac{d(\xi)^2T_1(\xi)_\xi T_1(\xi)_{\xi\xi}\left(\frac{d(\xi)T_0(\xi)_{\xi\xi}+\eta(\xi)T_1(\xi)}{\gamma(\xi)T_1(\xi)}\right)_\xi}{\gamma(\xi)T_1(\xi)^2} - \frac{d(\xi)^2T_1(\xi)_\xi T_0(\xi)_{\xi\xi}\left(\frac{d(\xi)T_1(\xi)_{\xi\xi}}{\gamma(\xi)T_1(\xi)}\right)_\xi}{54\,\gamma(\xi)T_1(\xi)^2}\\ & +\frac{1}{18}\frac{d(\xi)^3T_1(\xi)_\xi T_0(\xi)_\xi T_1(\xi)_{\xi\xi}^2}{T_1(\xi)^4\gamma(\xi)^2} + \frac{1}{9}\frac{d(\xi)^3T_1(\xi)_\xi^2T_1(\xi)_{\xi\xi}T_0(\xi)_{\xi\xi}}{T_1(\xi)^4\gamma(\xi)^2} - \frac{1}{36}\frac{d(\xi)^2T_1(\xi)_{\xi\xi}^2\eta(\xi)}{\gamma(\xi)^2T_1(\xi)^2}\\ & -\frac{1}{27}\frac{d(\xi)T_1(\xi)_\xi\eta(\xi)\left(\frac{d(\xi)T_1(\xi)_{\xi\xi}}{\gamma(\xi)T_1(\xi)}\right)_\xi}{\gamma(\xi)T_1(\xi)} - \frac{1}{36}\frac{d(\xi)^3T_1(\xi)_{\xi\xi}^2T_0(\xi)_{\xi\xi}}{T_1(\xi)^3\gamma(\xi)^2},\end{aligned} \tag{D2}$$

$$\begin{aligned}D_4(\xi) = {}& -\frac{1}{3}\frac{d(\xi)^2T_1(\xi)_\xi^2T_1(\xi)_{\xi\xi}\rho_1(\xi)}{T_1(\xi)^3\gamma(\xi)} + \frac{2}{9}\frac{d(\xi)^2T_1(\xi)_\xi^2T_0(\xi)_{\xi\xi}\eta(\xi)}{T_1(\xi)^3\gamma(\xi)^2}\\ & -\frac{1}{18}\frac{d(\xi)^2T_0(\xi)_\xi T_1(\xi)_{\xi\xi}\left(\frac{d(\xi)T_0(\xi)_{\xi\xi}+\eta(\xi)T_1(\xi)}{\gamma(\xi)T_1(\xi)}\right)_\xi}{\gamma(\xi)T_1(\xi)^2} + \frac{1}{3}\frac{d(\xi)^2T_1(\xi)_\xi T_1(\xi)_{\xi\xi}\rho_1(\xi)_\xi}{\gamma(\xi)T_1(\xi)^2}\\ & -\frac{1}{9}\frac{d(\xi)^2T_1(\xi)_\xi T_0(\xi)_{\xi\xi}\left(\frac{d(\xi)T_0(\xi)_{\xi\xi}+\eta(\xi)T_1(\xi)}{\gamma(\xi)T_1(\xi)}\right)_\xi}{\gamma(\xi)T_1(\xi)^2} + \frac{1}{36}\frac{d(\xi)^3T_0(\xi)_\xi^2T_1(\xi)_{\xi\xi}^2}{T_1(\xi)^4\gamma(\xi)^2} - \frac{1}{9}\frac{d(\xi)^2T_1(\xi)_{\xi\xi}T_0(\xi)_{\xi\xi}\eta(\xi)}{\gamma(\xi)^2T_1(\xi)^2}\\ & +\frac{1}{9}\frac{d(\xi)T_1(\xi)_\xi\rho_1(\xi)\left(\frac{d(\xi)T_1(\xi)_{\xi\xi}}{\gamma(\xi)T_1(\xi)}\right)_\xi}{T_1(\xi)} + \frac{1}{9}\frac{d(\xi)T_1(\xi)_\xi^2\eta(\xi)^2}{\gamma(\xi)^2T_1(\xi)^2} - \frac{\sqrt{2}d(\xi)^2T_1(\xi)_{\xi\xi}^2}{144\,\nu\,\gamma(\xi)T_1(\xi)}\\ & +\frac{2}{9}\frac{d(\xi)^3T_1(\xi)_\xi T_0(\xi)_\xi T_1(\xi)_{\xi\xi}T_0(\xi)_{\xi\xi}}{T_1(\xi)^4\gamma(\xi)^2} + \frac{2}{9}\frac{d(\xi)^2T_1(\xi)_\xi T_0(\xi)_\xi T_1(\xi)_{\xi\xi}\eta(\xi)}{T_1(\xi)^3\gamma(\xi)^2}\\ & +\frac{1}{9}\frac{d(\xi)^3T_1(\xi)_\xi^2T_0(\xi)_{\xi\xi}^2}{T_1(\xi)^4\gamma(\xi)^2} + \frac{1}{12}\frac{d(\xi)^2T_1(\xi)_{\xi\xi}^2\rho_1(\xi)}{\gamma(\xi)T_1(\xi)^2} - \frac{1}{18}\frac{d(\xi)^3T_1(\xi)_{\xi\xi}T_0(\xi)_{\xi\xi}^2}{T_1(\xi)^3\gamma(\xi)^2} - \frac{1}{18}\frac{d(\xi)T_1(\xi)_{\xi\xi}\eta(\xi)^2}{\gamma(\xi)^2T_1(\xi)}\\ & -\frac{1}{9}\frac{d(\xi)T_1(\xi)_\xi\eta(\xi)\left(\frac{d(\xi)T_0(\xi)_{\xi\xi}+\eta(\xi)T_1(\xi)}{\gamma(\xi)T_1(\xi)}\right)_\xi}{\gamma(\xi)T_1(\xi)} - \frac{1}{27}\frac{d(\xi)\eta(\xi)T_0(\xi)_\xi\left(\frac{d(\xi)T_1(\xi)_{\xi\xi}}{\gamma(\xi)T_1(\xi)}\right)_\xi}{\gamma(\xi)T_1(\xi)},\end{aligned} \tag{D3}$$

$$\begin{aligned}D_3(\xi) = {}& \frac{2}{9}\frac{d(\xi)^3T_1(\xi)_\xi T_0(\xi)_\xi T_0(\xi)_{\xi\xi}^2}{T_1(\xi)^4\gamma(\xi)^2} - \frac{1}{9}\frac{d(\xi)T_0(\xi)_\xi\eta(\xi)\left(\frac{d(\xi)T_0(\xi)_{\xi\xi}+\eta(\xi)T_1(\xi)}{\gamma(\xi)T_1(\xi)}\right)_\xi}{\gamma(\xi)T_1(\xi)}\\ & +\frac{2}{9}\frac{d(\xi)T_1(\xi)_\xi T_0(\xi)_\xi\eta(\xi)^2}{T_1(\xi)^2\gamma(\xi)^2} + \frac{1}{9}\frac{d(\xi)T_0(\xi)_\xi\rho_1(\xi)\frac{d(\xi)T_1(\xi)_{\xi\xi}}{\gamma(\xi)T_1(\xi)}_\xi}{T_1(\xi)} - \frac{1}{9}\frac{d(\xi)^2T_0(\xi)_{\xi\xi}^2\eta(\xi)}{T_1(\xi)^2\gamma(\xi)^2} + \frac{1}{6}\frac{T_1(\xi)_\xi d(\xi)T_1(\xi)_{\xi\xi}}{\gamma(\xi)T_1(\xi)^2}\\ & -\frac{d(\xi)T_1(\xi)_{\xi\xi}}{\gamma(\xi)T_1(\xi)}_\xi - \frac{1}{9}\frac{d(\xi)T_0(\xi)_{\xi\xi}\eta(\xi)^2}{\gamma(\xi)^2T_1(\xi)} - \frac{1}{27}\frac{\eta(\xi)^3}{\gamma(\xi)^2} + \frac{1}{3}\frac{d(\xi)^2T_0(\xi)_\xi T_1(\xi)_{\xi\xi}\rho_1(\xi)_\xi}{\gamma(\xi)T_1(\xi)^2} + \frac{1}{3}\frac{d(\xi)^2T_1(\xi)_\xi T_1(\xi)_{\xi\xi}\rho_0(\xi)_\xi}{\gamma(\xi)T_1(\xi)^2}\\ & +\frac{2}{3}\frac{d(\xi)^2T_1(\xi)_\xi T_0(\xi)_{\xi\xi}\rho_1(\xi)_\xi}{\gamma(\xi)T_1(\xi)^2} - \frac{\sqrt{2}d(\xi)T_1(\xi)_{\xi\xi}\eta(\xi)}{648\,\gamma(\xi)\nu} - \frac{2}{3}\frac{d(\xi)T_1(\xi)_\xi^2\eta(\xi)\rho_1(\xi)}{\gamma(\xi)T_1(\xi)^2} + \frac{4}{9}\frac{d(\xi)^2T_1(\xi)_\xi T_0(\xi)_\xi T_0(\xi)_{\xi\xi}\eta(\xi)}{T_1(\xi)^3\gamma(\xi)^2}\\ & -\frac{2}{3}\frac{d(\xi)^2T_1(\xi)_\xi T_0(\xi)_\xi T_1(\xi)_{\xi\xi}\rho_1(\xi)}{T_1(\xi)^3\gamma(\xi)} - \frac{1}{36}\frac{\sqrt{2}d(\xi)^2T_1(\xi)_{\xi\xi}T_0(\xi)_{\xi\xi}}{\gamma(\xi)T_1(\xi)\nu} + \frac{1}{3}\frac{T_1(\xi)_\xi d(\xi)\rho_1(\xi)\left(\frac{d(\xi)T_0(\xi)_{\xi\xi}+\eta(\xi)T_1(\xi)}{\gamma(\xi)T_1(\xi)}\right)_\xi}{T_1(\xi)}\end{aligned}$$

$$
\begin{aligned}
&-\frac{2}{3}\frac{d(\xi)^2T_1(\xi)_\xi^2T_0(\xi)_{\xi\xi}\rho_1(\xi)}{T_1(\xi)^3\gamma(\xi)}+\frac{1}{9}\frac{d(\xi)^2T_0(\xi)_\xi^2T_1(\xi)_{\xi\xi}\eta(\xi)}{T_1(\xi)^3\gamma(\xi)^2}+\frac{1}{3}\frac{d(\xi)^2T_1(\xi)_{\xi\xi}T_0(\xi)_{\xi\xi}\rho_1(\xi)}{\gamma(\xi)T_1(\xi)^2}\\
&+\frac{1}{3}\frac{d(\xi)T_1(\xi)_{\xi\xi}\eta(\xi)\rho_1(\xi)}{\gamma(\xi)T_1(\xi)}+\frac{1}{9}\frac{d(\xi)^3T_0(\xi)_\xi^2T_1(\xi)_{\xi\xi}T_0(\xi)_{\xi\xi}}{T_1(\xi)^4\gamma(\xi)^2}+\frac{2}{3}\frac{T_1(\xi)_\xi d(\xi)\eta(\xi)\rho_1(\xi)_\xi}{\gamma(\xi)T_1(\xi)}\\
&-\frac{1}{9}\frac{d(\xi)^2T_0(\xi)_\xi T_0(\xi)_{\xi\xi}\left(\frac{d(\xi)T_0(\xi)_{\xi\xi}+\eta(\xi)T_1(\xi)}{\gamma(\xi)T_1(\xi)}\right)_\xi}{\gamma(\xi)T_1(\xi)^2}-\frac{1}{27}\frac{d(\xi)^3T_0(\xi)_{\xi\xi}^3}{T_1(\xi)^3\gamma(\xi)^2}-\frac{1}{18}\frac{d(\xi)T_1(\xi)_{\xi\xi}}{\gamma(\xi)T_1(\xi)},
\end{aligned}
\tag{D4}
$$

$$
\begin{aligned}
D_2(\xi)=&\frac{1}{3}\frac{\eta(\xi)^2\rho_1(\xi)}{\gamma(\xi)}+\frac{1}{3}\frac{d(\xi)T_0(\xi)_\xi\rho_1(\xi)\left(\frac{d(\xi)T_0(\xi)_{\xi\xi}+\eta(\xi)T_1(\xi)}{\gamma(\xi)T_1(\xi)}\right)_\xi}{T_1(\xi)}\\
&+\frac{2}{3}\frac{d(\xi)T_0(\xi)_{\xi\xi}\eta(\xi)\rho_1(\xi)}{\gamma(\xi)T_1(\xi)}-\frac{1}{3}\frac{d(\xi)^2T_0(\xi)_\xi^2T_1(\xi)_{\xi\xi}\rho_1(\xi)}{T_1(\xi)^3\gamma(\xi)}+\frac{2}{9}\frac{d(\xi)^2T_0(\xi)_\xi^2T_0(\xi)_{\xi\xi}\eta(\xi)}{T_1(\xi)^3\gamma(\xi)^2}\\
&-\frac{1}{6}\frac{d(\xi)T_0(\xi)_{\xi\xi}+\eta(\xi)T_1(\xi)}{\gamma(\xi)T_1(\xi)}-\frac{1}{36}\frac{T_1(\xi)\sqrt{2}\eta(\xi)^2}{\nu\,\gamma(\xi)}+\frac{1}{12}\frac{\sqrt{2}d(\xi)T_1(\xi)_{\xi\xi}\rho_1(\xi)}{\nu}+\frac{1}{6}\frac{T_0(\xi)_\xi d(\xi)T_1(\xi)_{\xi\xi}}{\gamma(\xi)T_1(\xi)^2}\\
&+\frac{1}{3}\frac{T_1(\xi)_\xi d(\xi)T_0(\xi)_{\xi\xi}}{\gamma(\xi)T_1(\xi)^2}-\frac{1}{6}\frac{d(\xi)T_0(\xi)_{\xi\xi}+\eta(\xi)T_1(\xi)}{\gamma(\xi)T_1(\xi)_\xi}+\frac{2}{3}\frac{d(\xi)T_1(\xi)_\xi\eta(\xi)\rho_0(\xi)_\xi}{\gamma(\xi)T_1(\xi)}+\frac{2}{3}\frac{d(\xi)T_0(\xi)_\xi\eta(\xi)\rho_1(\xi)_\xi}{\gamma(\xi)T_1(\xi)}\\
&+\frac{2}{3}\frac{d(\xi)^2T_1(\xi)_\xi T_0(\xi)_{\xi\xi}\rho_0(\xi)_\xi}{\gamma(\xi)T_1(\xi)^2}-\frac{1}{36}\frac{\sqrt{2}d(\xi)^2T_0(\xi)_{\xi\xi}^2}{\nu\,\gamma(\xi)T_1(\xi)}-\frac{1}{18}\frac{\sqrt{2}d(\xi)T_0(\xi)_{\xi\xi}\eta(\xi)}{\nu\,\gamma(\xi)}\\
&+\frac{1}{3}\frac{d(\xi)^2T_0(\xi)_\xi T_1(\xi)_{\xi\xi}\rho_0(\xi)_\xi}{\gamma(\xi)T_1(\xi)^2}+\frac{2}{3}\frac{d(\xi)^2T_0(\xi)_\xi T_0(\xi)_{\xi\xi}\rho_1(\xi)_\xi}{\gamma(\xi)T_1(\xi)^2}+\frac{1}{3}\frac{d(\xi)^2T_0(\xi)_{\xi\xi}^2\rho_1(\xi)}{\gamma(\xi)T_1(\xi)^2}-\frac{1}{2}\frac{d(\xi)T_1(\xi)_{\xi\xi}\rho_1(\xi)^2}{T_1(\xi)}\\
&+\frac{d(\xi)T_1(\xi)_\xi^2\rho_1(\xi)^2}{T_1(\xi)^2}+\frac{1}{3}\frac{T_1(\xi)_\xi\eta(\xi)}{\gamma(\xi)T_1(\xi)}-\frac{4}{3}\frac{d(\xi)^2T_1(\xi)_\xi T_0(\xi)_\xi T_0(\xi)_{\xi\xi}\rho_1(\xi)}{T_1(\xi)^3\gamma(\xi)}\\
&-\frac{4}{3}\frac{d(\xi)T_1(\xi)_\xi T_0(\xi)_\xi\eta(\xi)\rho_1(\xi)}{\gamma(\xi)T_1(\xi)^2}+\frac{1}{9}\frac{d(\xi)T_0(\xi)_\xi^2\eta(\xi)^2}{T_1(\xi)^2\gamma(\xi)^2}-2\frac{d(\xi)T_1(\xi)_\xi\rho_1(\xi)\rho_1(\xi)_\xi}{T_1(\xi)}+\frac{1}{9}\frac{d(\xi)^3T_0(\xi)_\xi^2T_0(\xi)_{\xi\xi}^2}{T_1(\xi)^4\gamma(\xi)^2},
\end{aligned}
\tag{D5}
$$

$$
\begin{aligned}
D_1(\xi)=&\frac{1}{6}\frac{\sqrt{2}d(\xi)T_0(\xi)_{\xi\xi}\rho_1(\xi)}{\nu}-2\frac{d(\xi)T_0(\xi)_\xi\rho_1(\xi)\rho_1(\xi)_\xi}{T_1(\xi)}+\frac{2}{3}\frac{d(\xi)^2T_0(\xi)_\xi T_0(\xi)_{\xi\xi}\rho_0(\xi)_\xi}{\gamma(\xi)T_1(\xi)^2}-\frac{2}{3}\frac{d(\xi)^2T_0(\xi)_\xi^2T_0(\xi)_{\xi\xi}\rho_1(\xi)}{T_1(\xi)^3\gamma(\xi)}\\
&+\frac{1}{6}\frac{T_1(\xi)\sqrt{2}\eta(\xi)\rho_1(\xi)}{\nu}-2\frac{d(\xi)T_1(\xi)_\xi\rho_1(\xi)\rho_0(\xi)_\xi}{T_1(\xi)}+2\frac{d(\xi)T_1(\xi)_\xi T_0(\xi)_\xi\rho_1(\xi)^2}{T_1(\xi)^2}-\frac{T_1(\xi)_\xi\rho_1(\xi)}{T_1(\xi)}+\rho_1(\xi)_\xi\\
&+\frac{1}{3}\frac{T_0(\xi)_\xi\eta(\xi)}{\gamma(\xi)T_1(\xi)}+\rho_1(\xi)-\eta(\xi)\rho_1(\xi)^2-\frac{d(\xi)T_0(\xi)_{\xi\xi}\rho_1(\xi)^2}{T_1(\xi)}+\frac{1}{3}\frac{d(\xi)T_0(\xi)_\xi T_0(\xi)_{\xi\xi}}{\gamma(\xi)T_1(\xi)^2}\\
&+\frac{2}{3}\frac{d(\xi)T_0(\xi)_\xi\eta(\xi)\rho_0(\xi)_\xi}{\gamma(\xi)T_1(\xi)}-\frac{2}{3}\frac{d(\xi)T_0(\xi)_\xi^2\eta(\xi)\rho_1(\xi)}{\gamma(\xi)T_1(\xi)^2},
\end{aligned}
\tag{D6}
$$

$$
\begin{aligned}
D_0(\xi)=&-2\frac{d(\xi)T_0(\xi)_\xi\rho_1(\xi)\rho_0(\xi)_\xi}{T_1(\xi)}-\frac{1}{4}\frac{\sqrt{2}\gamma(\xi)T_1(\xi)\rho_1(\xi)^2}{\nu}+\frac{1}{3}\frac{d(\xi)T_1(\xi)_{\xi\xi}}{T_1(\xi)}\\
&+\frac{d(\xi)T_0(\xi)_\xi^2\rho_1(\xi)^2}{T_1(\xi)^2}-\frac{T_0(\xi)_\xi\rho_1(\xi)}{T_1(\xi)}+\gamma(\xi)\rho_1(\xi)^3.
\end{aligned}
\tag{D7}
$$

APPENDIX E: THE FINITE DIFFERENCE FORMULAE FOR THE DERIVATIVES

$$
\begin{aligned}
\left[\frac{\partial^2u(\xi,\tau)}{\partial\xi^2}\right]_{\xi=n\Delta\xi}&=\frac{u_{n+1}(\tau)-2u_n(\tau)+u_{n-1}(\tau)}{\Delta\xi^2}+0(\Delta\xi^2),\\
\left[\frac{\partial u(\xi,\tau)}{\partial\xi}\right]_{\xi=n\Delta\xi}&=\frac{u_{n+1}(\tau)-u_{n-1}(\tau)}{2\Delta\xi}+0(\Delta\xi^2),
\end{aligned}
\tag{E1}
$$

$$
\begin{aligned}
\left[\frac{\partial^2v(\xi,\tau)}{\partial\xi^2}\right]_{\xi=n\Delta\xi}&=\frac{v_{n+1}(\tau)-2v_n(\tau)+v_{n-1}(\tau)}{\Delta\xi^2}+0(\Delta\xi^2),\\
\left[\frac{\partial v(\xi,\tau)}{\partial\xi}\right]_{\xi=n\Delta\xi}&=\frac{v_{n+1}(\tau)-v_{n-1}(\tau)}{2\Delta\xi}+0(\Delta\xi^2),
\end{aligned}
\tag{E2}
$$

where

$$\begin{aligned} u_n(\tau) &\equiv u(n\Delta\xi,\tau) \\ u_{n-1}(\tau) &\equiv u((n-1)\Delta\xi,\tau) \\ u_{n+1}(\tau) &\equiv f(u_n(\tau),u_{n-1}(\tau),v_n(\tau)) \end{aligned} \tag{E3}$$

$$\begin{aligned} v_n(\tau) &\equiv v(n\Delta\xi,\tau) \\ v_{n-1}(\tau) &\equiv v((n-1)\Delta\xi,\tau) \\ v_{n+1}(\tau) &\equiv f(v_n(\tau),v_{n-1}(\tau),u_n(\tau)) \end{aligned} \tag{E4}$$

[1] N. Engheta and M. W. Kowarz, J. Appl. Phys. **67**, 639 (1990).
[2] V. Prelog, Science **193**, 17 (1976).
[3] T. Verbit, G. Koeckelberghs, and B. Champagne, Opt. Mater. Express **4**, 2663 (2014).
[4] S. B. Singham, J. Chem. Phys. **87**, 1873 (1987).
[5] R. T. Co, K. Harigaya, and Y. Nomura, Phys. Rev. Lett. **118**, 101801 (2017).
[6] P. L. Guennec, J. Math. Phys. **41**, 5954 (2000).
[7] E. Yomba and G.-A. Zakeri, Chaos **26**, 083115 (2016).
[8] P. K. Choudhury and T. Yoshino, Optik **113**, 89 (2002).
[9] C. Rizza, A. D. DiFalco, M. Scalora, and A. Ciattoni, Phys. Rev. Lett. **115**, 057401 (2015)
[10] N. Akhmediev and E. Pelinovsky, Eur. Phys. J. Special Topics **185**, 1 (2010).
[11] B. Frisquet *et al.*, Sci. Rep. **6**, 20785 (2016).
[12] J. M. Dudley, F. Dias, M. Erkintalo, and G. Genty, Nat. Photonics **8**, 755 (2014).
[13] D. R. Solli, C. Ropers, P. Koonath, and B. Jalali, Nature (London) **450**, 1054 (2007).
[14] D. Buccoliero, H. Steffensen, H. Ebendorff-Heidepriem, T. M. Monro, and O. Bang, Opt. Express **19**, 17973 (2011).
[15] P. Muller, C. Garrett, and A. Osborne, Oceanography **18**, 66 (2005).
[16] Y. V. Bludov, V. V. Konotop, and N. Akhmediev, Opt. Lett. **34**, 3015 (2009).
[17] Y. V. Bludov, V. V. Konotop, and N. Akhmediev, Eur. Phys. J.: Spec. Top. **185**, 169 (2010).
[18] Y. V. Bludov, V. V. Konotop, and N. Akhmediev, Phys. Rev. A **80**, 033610 (2009).
[19] S. Loomba, H. Kaur, R. Gupta, C. N. Kumar, and T. S. Raju, Phys. Rev. E **89**, 052915 (2014).
[20] Y. V. Bludov, R. Driben, V. V. Konotop, and B. A. Malomed, J. Opt. **15**, 064010 (2013).
[21] L. Wen, L. Li, Z. D. Li, S. W. Song, X. F. Zhang, and W. M. Liu, Eur. Phys. J. D **64**, 473 (2011).
[22] Z. Yan, Commun. Theor. Phys. **54**, 947 (2010).
[23] J. M. Soto-Crespo, N. Devine, and N. Akhmediev, Phys. Rev. Lett. **116**, 103901 (2016).
[24] M. Onorato, S. Residori, U. Bortolozzo, A. Montina, and F. T. Arecchi, Phys. Rep. **528**, 47 (2013).
[25] A. Slunyaev, Eur. Phys. J. Spec. Top. **185**, 67 (2010).
[26] C. Kharif and J. Touboul, Eur. Phys. J. Spec. Top. **185**, 159 (2010).
[27] G. P. Agrawal, *Nonlinear Fiber Optics*, 2nd ed. (Acdemic Press, New York, 1995).
[28] *Optical Fiber Communications III*, edited by I. P. Kaminow and T. L. Koch (Academic Press, New York, 1997).
[29] L. J. Richardson, W. Forysiak, and N. J. Doran, IEEE Photonics Technol. Lett. **13**, 209 (2001).
[30] F. Baronio, M. Conforti, A. Degasperis, S. Lombardo, M. Onorato, and S. Wabnitz, Phys. Rev. Lett. **113**, 034101 (2014).
[31] C. Bonatto, M. Feyereisen, S. Barland, M. Giudici, C. Masoller, J. R. R. Leite, and J. R. Tredicce, Phys. Rev. lett. **107**, 053901 (2011).
[32] A. Chabchoub, N. P. Hoffmann, and N. Akhmediev, Phys. Rev. Lett. **106**, 204502 (2011).
[33] H. Bailung, S. K. Sharma, and Y. Nakamura, Phys. Rev. Lett. **107**, 255005 (2011).
[34] C. Lecaplain, Ph. Grelu, J. M. Soto-Crespo, and N. Akhmediev, Phys. Rev. Lett. **108**, 233901 (2012).
[35] G. Baruch, G. Fibich, and S. Tsynkov, Opt. Express **16**, 13323 (2008).
[36] P. Chamorro-Posada, G. S. McDonald, and G. H. C. New, J. Mod. Opt. **45**, 1111 (1998).
[37] P. Chamorro-Posada, G. S. McDonald, and G. H. C. New, Opt. Commun. **192**, 1 (2001).
[38] S. I. Fewo, H. Moussambi, and T. C. Kofane, Phys. Scr. **84**, 035002 (2011).
[39] F. Biancalana and C. Creatore, Opt. Express **16**, 14882 (2008).
[40] D. H. Peregrine, J. Aust. Math. Soc. Series B, Appl. Math. **25**, 16 (1983).
[41] S. Chen, J. M. Soto-Crespo, and Ph. Grelu, Opt. Express **23**, 349 (2015).
[42] J. He, L. Wang, L. Li, K. Porsezian, and R. Erdélyi, Phys. Rev. E **89**, 062917 (2014).
[43] F. Baronio, A. Degasperis, M. Conforti, and S. Wabnitz, Phys. Rev. Lett. **109**, 044102 (2012).
[44] F. Baronio, M. Conforti, A. Degasperis, and S. Lombardo, Phys. Rev. Lett. **111**, 114101 (2013).
[45] S. Chen, J. M. Soto-Crespo, and Ph. Grelu, Phys. Rev. E **90**, 033203 (2014).
[46] L. C. Zhao and J. Liu, Phys. Rev. E **87**, 013201 (2013).
[47] A. T. Avelar, D. Bazeia, and W. B. Cardoso, Phys. Rev. E **79**, 025602 (2009).

[48] N. Akhmediev, A. Ankiewicz, and J. M. Soto-Crespo, Phys. Rev. E **80**, 026601 (2009).
[49] J. Li, T. Xu, X.-H. Meng, Y.-X. Zang, H.-Q. Zhanga, and B. Tiang, J. Math. Anal. Appl. **336**, 1443 (2007).
[50] A. Degasperis and S. Lombardo, J. Phys. A **40**, 961 (2007).
[51] A. Degasperis and S. Lombardo, J. Pyhs. A **42**, 385206 (2009).
[52] A. Degasperis and S. Lombardo, Phys. Rev. E **88**, 052914 (2013).
[53] F. Baronio, S. Chen, P. Grelu, S. Wabnitz, and M. Conforti, Phys. Rev. A **91**, 033804 (2015).
[54] S. Chen, J. M. Soto-Crespo, F. Baronio, P. Grelu, and D. Mihalache, Opt. Express **24**, 15251 (2016).
[55] Z. Yan and C. Dai, J. Opt. **15**, 064012 (2013).
[56] G. W. Bluman and S. Kumei, *Symmetries and Differential Equations* (Springer, New York, 1989).
[57] G. W. Bluman and Z. Y. Yan, Eur. J. Appl. Math. **16**, 239 (2005).
[58] Z. Yan, V. V. Konotop, and N. Akhmediev, Phys. Rev. E **82**, 036610 (2010).
[59] W.-P. Zhong, M. R. Belic, and T. Huang, Phys. Rev. E **87**, 065201 (2013).
[60] A. Ankiewicz, J. M. Soto-Crespo, and N. Akhmediev, Phys. Rev. E **81**, 046602 (2010).
[61] E. N. Tsoy, A. Ankiewicz, and N. Akhmediev, Phys. Rev. E **73**, 036621 (2006).
[62] N. Akhmediev, V. M. Eleonskii, and N. E. Kulagin, Sov. Phys. JETP **89**, 1542 (1985).
[63] H. Torres-Silva and M. Zamorano, Math. Comput. Sim. **62**, 149 (2003).
[64] B. Bai, Y. Svirko, J. Turunen, and T. Vallius, Phys. Rev. A **76**, 023811 (2007).
[65] B. Bai, J. Laukkanen, A. Lehmuskero, and J. Turunen, Phys. Rev. B **81**, 115424 (2010).